Molecular representation of benzene and phenol secondary organic aerosols

Aurélien Le Bayon[1], Aliisa Ojala[2], Siddharth Iyer[2], Zhizhao Wang[3], Victor Lannuque[4], Florian Couvidat[4], Raluca Ciuraru[5], and Karine Sartelet[1]

[1]CEREA, Ecole nationale des ponts et chaussées, EDF R&D, Institut Polytechnique de Paris, IPSL, 77455 Marne-la-vallée, France
[2]Aerosol Physics Laboratory, Tampere University, 33720 Tampere, Finland
[3]College of Engineering Center for Environmental Research and Technology (CE-CERT), University of California, Riverside, CA 92521, USA
[4]Institut National de l'Environnement Industriel et des Risques, 60550 Verneuil-en-Halatte, France
[5]ECOSYS, University Paris-Saclay, INRAE, AgroParisTech, 91120 Palaiseau, France

Correspondence: Aurélien Le Bayon (aurelien.le-bayon@enpc.fr), Siddharth Iyer (siddharth.iyer@tuni.fi), and Karine Sartelet (karine.sartelet@enpc.fr)

Abstract.

Recent experimental and theoretical work has highlighted missing pathways in the oxidation of aromatic compounds, with consequences for the formation of highly oxygenated products relevant to secondary organic aerosol (SOA) formation. In this study we develop an updated, quasi-explicit oxidation mechanism for benzene based on Master Chemical Mechanism (MCM) v3.3.1, extended to represent key multi-generation chemistry. Quantum chemical calculations are used to derive the formation and evolution of geminal-diol bicyclic peroxy radicals and to parameterize the subsequent molecular rearrangements. The mechanism further incorporates autoxidation sequences previously developed for peroxy and alkoxy radicals, successive OH additions and cyclic epoxides formation. This approach enables a more mechanistic description of aromatic oxidation leading to highly oxygenated, low-volatility products. The mechanism is evaluated using box-model simulations against a set of chamber experiments conducted under various conditions. Simulated aerosol concentrations agree well with observations and emphasize the dominant contribution of the newly implemented pathways. The quasi-explicit mechanism is subsequently reduced using the GENerator of reduced Organic Aerosol mechanisms (GENOA), resulting in a semi-explicit mechanism reduced to 1 % of its original number of species while reproducing SOA mass with a mean error of 3.9 % relative to the quasi-explicit scheme. Using the validated reduced mechanism, zero-dimensional simulations under contrasted atmospheric conditions are conducted to estimate the SOA compounds that are formed in the early stages of oxidation and those that dominate the system at later stages.

1 Introduction

Volatile organic compounds (VOCs) play an important role in the formation of secondary organic aerosols (SOA). In the atmosphere, these compounds may react with oxidants such as OH, O_3 and NO_3, leading to the formation of more functionalized

organic species (Jacob, 1999; Kroll and Seinfeld, 2008). These newly formed species may have a lower saturation vapor pressure and are more likely to participate to the formation and growth of SOA (Pankow, 1994), which have multiple impacts on health (Mauderly and Chow, 2008; Pope et al., 2002) and environment (Kanakidou et al., 2005).

Aromatic compounds account for a significant proportion of anthropogenic VOCs (Reimann and Lewis, 2007). Benzene, the simplest aromatic compound, is considered a carcinogen and endocrine disruptor (Baan et al., 2009), and it can affect the circulatory system or lead to the development of chronic diseases (Lan et al., 2004; Bahadar et al., 2014). This compound is emitted by many sources: traffic, cigarette smoke, and industrial solvent use, particularly in sectors such as textiles, pesticides and pharmaceuticals (Weisel, 2010). Phenol is the main product of benzene oxidation by the hydroxyl radical. It may also be primarily emitted by numerous primary sources in the atmosphere, such as biomass burning, traffic exhaust and manure spreading in agriculture (Mohr et al., 2013; Sun et al., 2008). Oxidation of benzene and phenol leads to the formation of functionalised products that may form SOA, including glyoxal and methylglyoxal (Jang et al., 2002).

In three-dimensional (3D) simulation models, the formation of SOA from a VOC precursor is usually parameterized based on yields derived from atmospheric simulation chamber experiments. Typical approaches include the two-compound Odum approach (Odum et al., 1996), the surrogate approach (Pun et al., 2006; Couvidat et al., 2012), or the volatility basis set (Donahue et al., 2006). While computationally efficient, these parameterizations do not explicitly resolve the molecular composition of the particle phase, or do so only for a limited number of representative compounds in the case of the surrogate approach (Couvidat et al., 2012; Majdi et al., 2019). To improve the representation of aerosol chemical composition and reduce reliance on empirical fitting, semi-explicit approaches are emerging (Wang et al., 2022; Luttkus et al., 2024; Wieser et al., 2024). These approaches selectively retain the main products and reaction pathways from explicit oxidation mechanisms, along with their subsequent degradation products.

Quasi-explicit oxidation schemes provide a comprehensive representation of atmospheric photooxidation products and reactions (Bloss et al., 2005; Aumont et al., 2005), but their complexity limits their use in 3D air-quality models. Hence Wang et al. (2022, 2023b) developed an algorithm to reduce quasi-explicit chemical mechanisms to sizes suitable for 3D atmospheric simulations, while conserving the predominant pathways and characteristics of SOA compounds. In this algorithm, called GENerator of reduced Organic Aerosol mechanism (GENOA), the main oxidation pathways are identified, accounting for radical chemistry, which has been shown to be crucial for monoterpenes (Wang et al., 2024). The SOA chemical composition is accurately represented in terms of functional groups (Wang et al., 2022), making it possible to capture interactions between compounds through non-ideality and partitioning into both organic and aqueous phases (Couvidat and Sartelet, 2015; Kim et al., 2019). Coupled to 3D air-quality models, the reduced mechanisms enable mapping of the molecular composition of SOA on multiple spatial scales, as demonstrated for terpenes at the European scale (Wang et al., 2024) and for toluene from regional to street-scale applications (Sartelet et al., 2024).

The Master Chemical Mechanism (MCM) (Jenkin et al., 2003; Bloss et al., 2005) is a quasi-explicit mechanism that accurately represents precursor degradation and formation of first-generation oxidation products (Calvert et al., 2002). However, based on the results of experimental studies on benzene oxidation (Nakao et al., 2011; Borrás and Tortajada-Genaro, 2012; Priestley et al., 2021; Cheng et al., 2021; Choi et al., 2024), several compounds and oxidation pathways are not included in

this scheme which especially underrepresents the formation of highly oxidized compounds and organonitrates, thus strongly impacting SOA formation. In recent years, experimental data analysis led to the identification of new oxidation pathways with adjustment of previously existing ones, to better represent the formation of specific compounds, such as nitrocatechol (Harrison et al., 2005) and the formation of observed fragmentation products, such as glyoxal and muconaldehyde (Wang et al., 2013) or ketene-enols and small carboxylic acids (Xu et al., 2020; Wang et al., 2020). An autoxidation mechanism was also developed for benzene, allowing for a better representation of several classes of compounds, such as peroxides and organonitrates (Pichelstorfer et al., 2024). Pathways related to the rearrangement of bicyclic peroxy radicals (BPR) are still missing, especially for geminal diol derived BPRs formed from the oxidation of phenol and catechol.

This work aims to construct a semi-explicit scheme for benzene oxidation that integrates the main SOA formation pathways relevant under atmospheric conditions. First, a quasi-explicit oxidation scheme is developed, incorporating recent advances in the understanding of benzene oxidation. This mechanism, based on the Master Chemical Mechanism and enriched by the state-of-the-art known oxidation routes, is presented in section 2. Quantum chemical calculations are then used to investigate the role of BPR rearrangements, which may be particularly relevant for geminal diols formed during the oxidation of phenol and catechol. Pathways related to BPR rearrangement are determined in section 3. Comparison with experimental data is used to validate the quasi-explicit scheme in section 4. The quasi-explicit scheme is reduced using GENOA for 3D atmospheric air-quality modeling by training over Europe in section 5. The relative influence of the different pathways for benzene and phenol SOA formation under atmospheric conditions is studied in section 6.

2 Benzene and phenol oxidation mechanism

2.1 The MCM near-explicit baseline

The quasi-explicit benzene oxidation mechanism developed in this work is based on the MCM v3.3.1 (Jenkin et al., 2003; Bloss et al., 2005) to which several oxidation pathways are added. The MCM scheme integrates 135 species and 334 reactions, initiated by the benzene oxidation by the hydroxyl radical. Three distinct compounds result from this first step, phenol from hydroxyl radical addition on the aromatic cycle, a BPR from the addition of OH and two O_2 and a dicarbonyl epoxide through OH and O_2 addition followed by ring opening.

2.2 Successive OH addition pathway

In addition to the H-abstraction from the hydroxyl group, OH can react with phenols via addition to the aromatic ring. In the benzene MCM scheme, two successive OH additions are represented, leading to the formation of two phenolic compounds, phenol and catechol (dihydroxybenzene). Owing to the electrophilic nature of the hydroxyl group, the kinetics of OH addition become increasingly important as the number of OH-substituted carbons on the aromatic ring increases (Atkinson et al., 2006). Following the work of Schwantes et al. (2017) on toluene oxidation, further OH addition is considered in the quasi-explicit scheme, leading to the formation of new phenolic compounds, tri, tetra and pentahydroxybenzene. These compounds further

react in the atmosphere and lead to the formation of BPRs through OH addition and O_2 addition, alkyl peroxides through RO_2 + HO_2 reactions and quinones formation through bicylic alkoxy radical degradation. The branching ratios used in the multi-hydroxylation pathway could be assumed to be the same as their methylated equivalent presented in Schwantes et al. (2017) for cresol, i.e., 7 % for H-abstraction and 93 % for addition. However, recent studies indicate a higher branching ratio for abstraction in the reaction of catechol with OH, Finewax et al. (2018) proposes an abstraction branching ratio of 30 % with an addition rate of 70 %. The kinetic constants are extracted from the MCM when available or calculated using the Structure-Activity Relationship (SAR) method implemented in the generator of explicit mechanisms GECKO-A (Generator for Explicit Chemistry and Kinetics in the Atmosphere) (Jenkin et al., 2018). For aromatic compounds, the kinetic constant is calculated based on the number of substituted carbons and the nature and position of the substituents on the aromatic ring (see example in Supplement S1). The reactions and compounds resulting from the successive hydroxylation of benzene are integrated into the quasi-explicit mechanism (see Supplement S2).

2.3 Peroxy and alkoxy radicals autoxidation pathway

Autoxidation, defined as successive intramolecular reactions followed at each step by O_2 addition reactions, results in the formation of peroxy radicals (RO_2) with high oxygenated content. Bimolecular reactions involving peroxy radicals may also lead to the formation of alkoxy radicals. Radical termination in the autoxidation cycle leads to the formation of organonitrates (reaction with NO), hydroperoxides (reaction with HO_2), carbonyl compounds and dialkyl peroxide dimers ($ROOR'$). These dimers are compounds of extremely low volatility and result from the accretion reactions between peroxy radicals $RO_2{-}R'O_2$ (Berndt et al., 2018).

The autoAPRAM framework developed by Pichelstorfer et al. (2024) allows to generate complete autoxidation mechanisms using specified alkoxy and peroxy radicals as input. Two sets of standard reaction types are implemented in the framework: the first set comprises twelve types of reactions specific to peroxy radicals, taking into account reactions with radicals (NO, HO_2, RO_2), possible autoxidation reactions (H-shift and O_2 addition), accretion reactions, alkoxy radical formation from bimolecular reactions and peroxy radical termination (Crounse et al., 2012; Bianchi et al., 2019; Orlando and Tyndall, 2012). The second set defines alkoxy radicals chemistry through three reactions and includes fragmentation, autoxidation and reactions forming closed shell products (see Supplement S9). These reaction sets are applied to each alkoxy and peroxy radical from the input scheme and each newly formed radical, generating the complete autoxidation mechanism.

Using the autoAPRAM framework with the peroxy and alkoxy radicals from the benzene MCM mechanism as input, the autoxidation mechanism generated in Pichelstorfer et al. (2024) comprises 869 species and 934 reactions. Over 85 % of these reactions stem from the accretion processes, as each peroxy radicals combination must be considered as a reaction. This mechanism is integrated in the quasi-explicit scheme to take into account the autoxidation processes initiated by the benzene MCM scheme.

2.4 Cyclic epoxide formation pathway

Epoxide compounds exhibit significant uptake in the particle phase, thus playing an important role in aerosol formation and growth (Piletic et al., 2013). For isoprene chemistry, epoxide formation is explained as the OH-oxidation of a carbon double bond neighboring a hydroperoxide group (Paulot et al., 2009; Lin et al., 2012). In a similar fashion, Fu et al. (2023) identified the oxidation pathways leading to the formation of cyclic epoxides from toluene. From electronic structure and kinetic calculations, OH oxidation of toluene-derived bicyclic peroxides (T-ROOH) and nitrates (T-RONO2) can lead to the formation of the cyclic epoxide, with a 56.1 % and 22.4 % yield respectively. Other competitive reaction pathways are discussed in Fu et al. (2023), leading to the formation of a ring-open epoxide with a 1.44 % yield as well as highly volatile C2-C4 dicarbonyls with a 42.4 % yield for T-ROOH. The oxidation of T-RONO2 essentially leads to the formation of light dicarbonyls (56.0 %), dicarbonyl retaining the O-O bridge (21.4 %) and the nitrated equivalent of the epoxide formed by T-ROOH (0.2 %). In the absence of further information for benzene, the branching ratios presented in Fu et al. (2023) are used for the OH oxidation of benzene-derived bicyclic peroxide and nitrate. Following the nomenclature of Fu et al. (2023), species introduced in the benzene oxidation scheme are named BEPOX, B-ROOH, and B-RONO2.. Minor oxidation pathways (<2 % yield) are not considered in the implemented mechanism. The compounds and adapted branching ratios involved in the formation of BEPOX are described in Fig. 1.

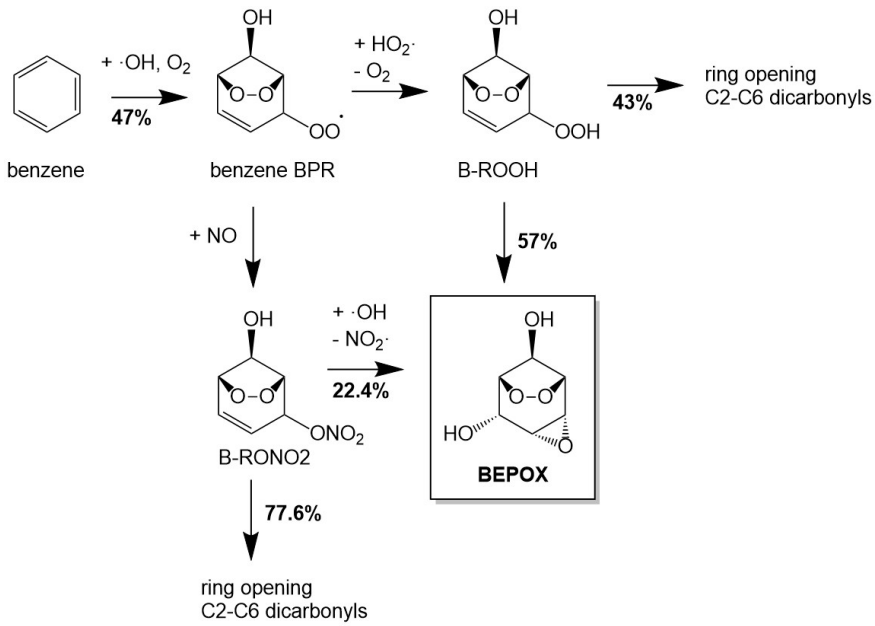

Figure 1. Formation of the cyclic epoxide BEPOX from B-ROOH and B-RONO2 oxidation and competing reaction pathways following the pathways suggested by Fu et al. (2023) for toluene.

2.5 Adaptation of existing pathways

The oxidation pathways proposed by MCM v3.3.1 for benzene have been updated based on recent experimental results and theoretical calculations. In MCM v3.3.1, the oxidation reaction of benzene by OH leads to the formation of phenol (53 %), of benzene-BPR (35.2 %) and of an open-chain epoxide (11.8 %). Experimentally, the epoxide is observed with a very low yield (Zaytsev et al., 2019; Xu et al., 2020) and epoxide compounds are rather formed from BPR pathways, as discussed in section 2.4. First generation epoxide formation is therefore removed from the quasi-explicit scheme and the branching ratio leading to the BPR formation is updated to 47 % (Xu et al., 2020).

In the benzene MCM scheme, the bicyclic alkoxy radical formed from benzene BPR is assumed to degrade exclusively via decomposition into glyoxal, butenedial, and furanone. However, a thermokinetic study conducted by Wang et al. (2020) demonstrated that an alternative H-shift pathway can compete with decomposition, leading to the formation of a ketene–enol intermediate. This intermediate rapidly oxidizes to formyl ketene, glyoxal, and formic acid. The same study also investigated butenedial oxidation, and identified the 3-carbon aldehyde acrolein as an additional degradation product. To better represent the bicyclic alkoxy radical degradation, oxidation schemes of ketenol (derived from Wang et al. (2020)) and acrolein (from MCM v3.3.1) are included in the quasi-explicit benzene scheme.

Due to their high level of functionalization and very low saturation vapor pressures, most end products resulting from the newly implemented pathways partition almost entirely into the particulate phase. For compounds whose volatility is high enough to allow their presence in both gas and particulate phases, loss reactions are implemented to prevent their accumulation. Following the approach used in Lannuque et al. (2023), degradation via photolysis and reactions with OH, NO, and NO_3 radicals are considered for these compounds without explicitly accounting for their oxidation products and using the SAR method to estimate their kinetic rate constants.

3 Rearrangement of the bicyclic peroxy radicals

3.1 Benzene BPR

Bicyclic peroxy radicals are key intermediates in the chemistry of aromatic compounds, formed through OH addition on the ring followed by O_2-additions. In the MCM scheme, benzene BPR forms a bicyclic alkoxy radical mainly through reaction with NO, being able to undergo ring-opening and ultimately forming C2 and C4 compounds, such as glyoxal, butenedial and furanone.

Non-cyclic compounds may also be formed from spontaneous rearrangement of BPR, as detailed in Iyer et al. (2023) for toluene. This process leads to the breakage of the peroxide bridge along one of the adjacent C-C bonds, linked to the OH functional group. Following ring-breakage, the ring-opened RO_2 undergoes two consecutive autoxidation cycles. A 1,6 H-shift from the -OH substituted carbon first leads to a resonance stabilized alkyl radical, that then rapidly adds O_2 to form a $C_6H_7O_7$ peroxy radical. This in turn has a 1,6 enolic H-shift, a reaction reported previously to be exceptionally fast (Peeters and Nguyen, 2012; Franzon et al., 2025), forming a $C_6H_7O_9$ peroxy radical. Its hydrogenation by reaction with HO_2 leads

to the formation of the main termination product of this cycle, the trihydroperoxide $C_6H_8O_9$. Due to its low saturation vapor pressure, it is mainly found in the particulate phase and further autoxidation reactions are not represented. The autoxidation sequence previously described and represented in Fig. 2 is implemented in the quasi-explicit oxidation scheme. The kinetic constants for benzene BPR rearrangement and further reactions are based on the thermodynamic calculations presented in Iyer et al. (2023).

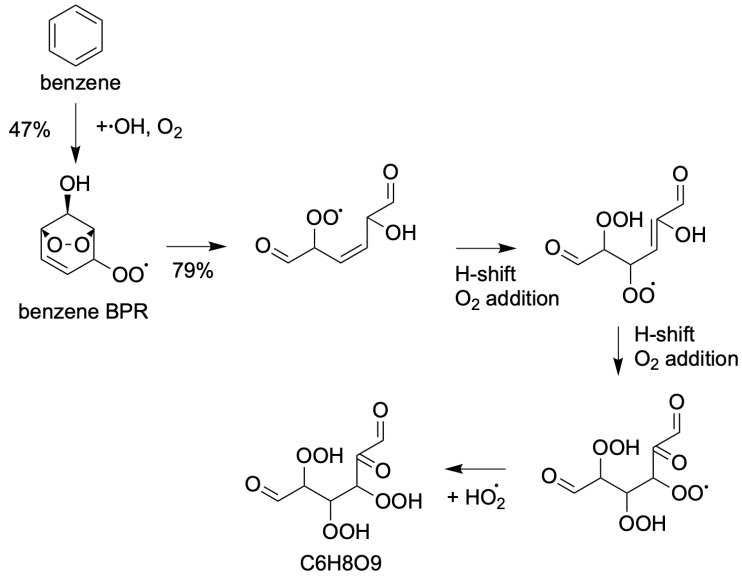

Figure 2. Simplified autoxidation pathway and termination of benzene BPR rearrangement as represented in the quasi-explicit mechanism.

3.2 Geminal diol BPR

In commonly used oxidation schemes, hydroxyl radical addition only occurs on non-substituted ring carbons, leading to the formation of vicinal diols. However, OH addition can also occur at already substituted carbons. This can lead to geminal diol BPRs that can undergo molecular rearrangement with rate constants that are several orders of magnitude higher compared to non-oxygenated aromatics. (Ojala et al., 2025). As a result, the oxidation of phenol and catechol via the geminal diol pathway can rapidly yield highly oxygenated organic molecules (HOM), including C_6 carboxylic acids and even diacids in the case of catechol. The yields of HOM via this pathway are a function of the initial OH addition yield, branching ratio to the formation of BPR intermediates, molecular rearrangement rate coefficient of the BPR and subsequent chemistry following molecular rearrangement. This means that the minor geminal diol BPR pathway can have a disproportionately high contribution to the SOA yield. Reaction rate constants and resulting product structures are determined using quantum chemical calculations, as is now detailed.

3.2.1 Quantum chemical calculations

The rate coefficients are calculated using multi-conformer transition state theory (MC-TST), with the equation:

$$k = \kappa \frac{k_b T}{h} \frac{\sum_i Q_i e^{\frac{-\Delta E_i}{k_b T}}}{\sum_j Q_j e^{\frac{-\Delta E_j}{k_b T}}} e^{\frac{-E_i - E_j}{k_b T}}$$

where k_b is the Boltzmann constant, T is the temperature, h is the Planck constant, Q_k are the partition functions and E_k are the energies. The MC-TST equation includes a Boltzmann weighted contribution of the partition functions of multiple low-lying conformers of the transition state and reactant. The index i refers to the transition states and j to the reactant, the summations runs over all relevant conformers and the energy differences in the sum refer to the energy difference in relation to the lowest energy conformer. The κ is the tunneling coefficient calculated with the Eckart tunneling method, which uses the energies of the optimized intrinsic reaction coordinate (IRC) endpoints and the magnitude of the imaginary frequency of the lowest energy transition state conformer. The quantum chemical calculations follow the steps detailed in Møller et al. (2016). Full conformer sampling of all studied molecules is performed with the Spartan '24 program using the MMFF method. Single-point calculations are performed for the conformers at the B3LYP/6-31+G(d) level of theory (henceforth denoted B3LYP) with structures within the cutoff of 5 kcal/mol in relation to the lowest energy conformer being selected for further optimization. If many conformers are present, an additional geometry optimization at the same B3LYP level is used, and conformers outside a 2 kcal/mol cutoff are rejected. Further density functional theory geometry optimization is done at ωB97X-D/aug-cc-pVTZ level of theory (denoted ωB97 level of theory), with the same level of theory used for the frequency calculation for determining the partition function. Transition states are found by first carrying out constrained optimizations of guess transition state structures, followed by unconstrained transition state optimizations using Gaussian 16 software, both at B3LYP level of theory. Conformer sampling, ωB97 optimization and frequency calculations are performed on the lowest energy conformers. Further refining at ROHF-ROCCSD(T)-F12a/VDZ-F12 (abbreviated F12) level of theory is done for the lowest energy conformers of all studied molecules, and the IRC endpoints, whereas ωB97 level of theory is used for the relative energies of the conformers. This has been shown to be a cost-effective way to calculate rate coefficients, where as calculating the F12 correction for all conformers increases notably the computational cost with diminishing benefits Møller et al. (2016). CCSD(T) corrections were not performed for H-shift reactions from OH groups, as the F12-level calculations for this reaction class have previously been shown to lead to artifact solutions (Møller et al., 2019).

3.2.2 Endocyclization branching ratios of the geminal diol mechanism

The formation of BPRs requires 5-member oxygen bridge formation over the location of the newly added OH group. Forming the bridge this way is important as the H-O interaction makes the endocyclization reaction competitive. This results in a delocalized alkyl radical, which forms a BPR with the addition of O_2. Ignoring chirality, one geminal diol BPR structure is possible for phenol due to the symmetry of the system, while two are possible for catechol. The endocyclization reactions and, consequently, the formation of geminal diol BPRs, compete with 1,5 H-shift reactions for phenol and catechol, and an additional HO_2 loss reaction for catechol specifically. This pathway leads to the formation of a closed shell $C_6H_6O_3$ compound

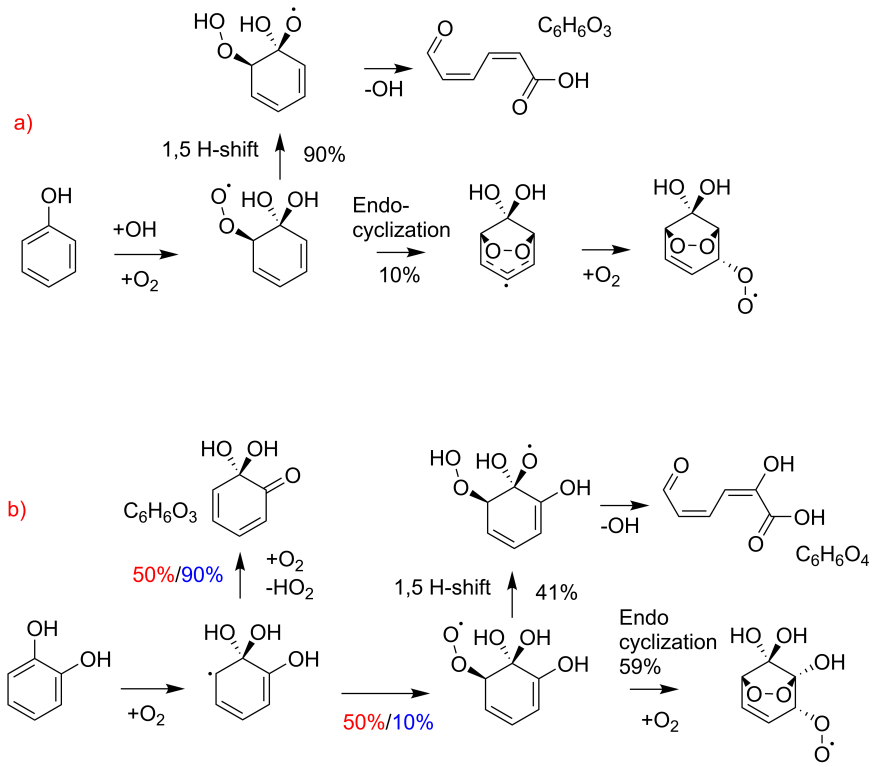

Figure 3. Endocyclization. a) for phenol and b) for catechol. Endocyclization has branching ratios of 10 % and 59 % for phenol and catechol respectively.

containing geminal diol and carbonyl functionalities. The 1,5 H-shift scheme is illustrated in Fig. 3, with the rates given in Table 1.

Table 1. Rate coefficients for the reactions relevant for endocyclization (s^{-1})

	Phenol	Catechol
1,5 H-shift	1.52	30.87
Endocyclization	0.17	44.68
Branching ratio	10.0 %	59.1 %

The endocyclization branching ratio is calculated from equation $BR_{path} = \frac{k_{path}}{k_{total}}$. The tunneling factor is subject to uncertainties due to the labile nature of the product alkyl radical, as discussed in Ojala et al. (2025). For this reason, a tunneling factor of 18.0 is used in analogy to para-cresol, yielding an endocyclization branching ratio of 10 %. For catechol, the alkyl radical is stable at the B3LYP level of theory and this is used for the tunneling calculations, yielding a branching ratio of 59 %.

Due to the asymmetry of the molecule, the O_2 addition to catechol can happen to two different locations and the subsequent chemistry is site-specific (see 3). The O_2 addition to the OH-substituted carbon leads to termination via HO_2 loss forming a closed shell carbonyl compound, hindering BPR formation. On the other hand, O_2 addition to the unsubstituted carbon in ortho position relative to the geminal diol carbon lead to endocyclization. The branching between the two O_2 addition sites cannot be accurately determined using quantum chemistry methods. To account for this, two scenarios were considered, corresponding to O_2 addition branching ratios of 10 % and 50 % to the pathway leading to endocyclization. Further details are provided regarding the mechanisms in Table 2 and a sensitivity analysis is conducted in section 4.5.4 regarding the endocyclization branching ratio.

3.2.3 Molecular rearrangement

Endocyclization is quickly followed by O_2 addition to form a geminal diol BPR, which can undergo a molecular rearrangement reaction as described previously for toluene and other non-oxygenated aromatic hydrocarbons in Iyer et al. (2023). Phenol has only one geminal diol BPR isomer due to the symmetry of the molecule, whereas catechol has two BPR isomers depending on which carbon the O_2 adds to. Both of these have different molecular rearrangement reaction rate coefficients that lead to two unique ring opened peroxy radicals. The molecular rearrangement reaction and the subsequent chemistry is shown in Fig. 4 for all of these.

The molecular rearrangement reaction can proceed in two ways, C_1 or C_2, depending on which of the two C-C bonds involved in the reaction is broken (Iyer et al., 2023; Ojala et al., 2025). The transition state for the C_1 pathway exhibits an intramolecular interaction between the -OO and -OH groups, reducing the reaction barrier of the rearrangement. In the presence of this interaction, the transition state for phenol tends to constantly optimize to C_1 regardless of the bond constraints used. In the case of catechol, both BPRs undergo molecular rearrangement only along one direction as shown in Fig. 4. We were unable to find the transition state for the other pathway for either BPR isomer, likely due to the fact that it leads to geminal diol intermediates that are energetically unfavorable.

The C_1 pathway for phenol yields a $C_6H_7O_6$ peroxy radical that can undergo a 1,6 aldehydic H-shift followed by O_2 addition to form a $C_6H_7O_8$ peroxy radical (Fig. 4 a). This can undergo H-scrambling between the hydroperoxy acyl peroxy and peroxy peroxoic acid radical forms, with the latter being thermodynamically more favoured (Knap and Jørgensen, 2017). Both forms behave identically in the current mechanism, as the volatility calculation assumes that the peroxy radicals react with HO_2 to form hydroperoxides. To simplify the mechanism in the model, the two catechol BPR isomers are treated as a single system, both with molecular rearrangement rate coefficients of 19.2 s^{-1}, leading to an equal 50% yields of ring opened peroxy radicals $C_6H_7O_7{-}a$ and $C_6H_7O_7{-}b$. The peroxy radical isomer from C_1 (Fig. 4 c) lacks an obvious labile H-atom and is unlikely to undergo further autoxidation under atmospheric conditions. This is different for the peroxy radical isomer that forms along C_2 (Fig. 4 b), which can undergo two rapid 1,6 H-shift, identical to those shown for benzene BPR in Fig. 4, to produce $C_6H_7O_{11}$ peroxy radicals. Note that a fraction of the alkyl radical following the first 1,6 H-shift could also terminate to a carbonyl compound by reacting with O_2. It is difficult to accurately estimate the branching between radical termination and further autoxidation, so we assume a 50:50 ratio here.

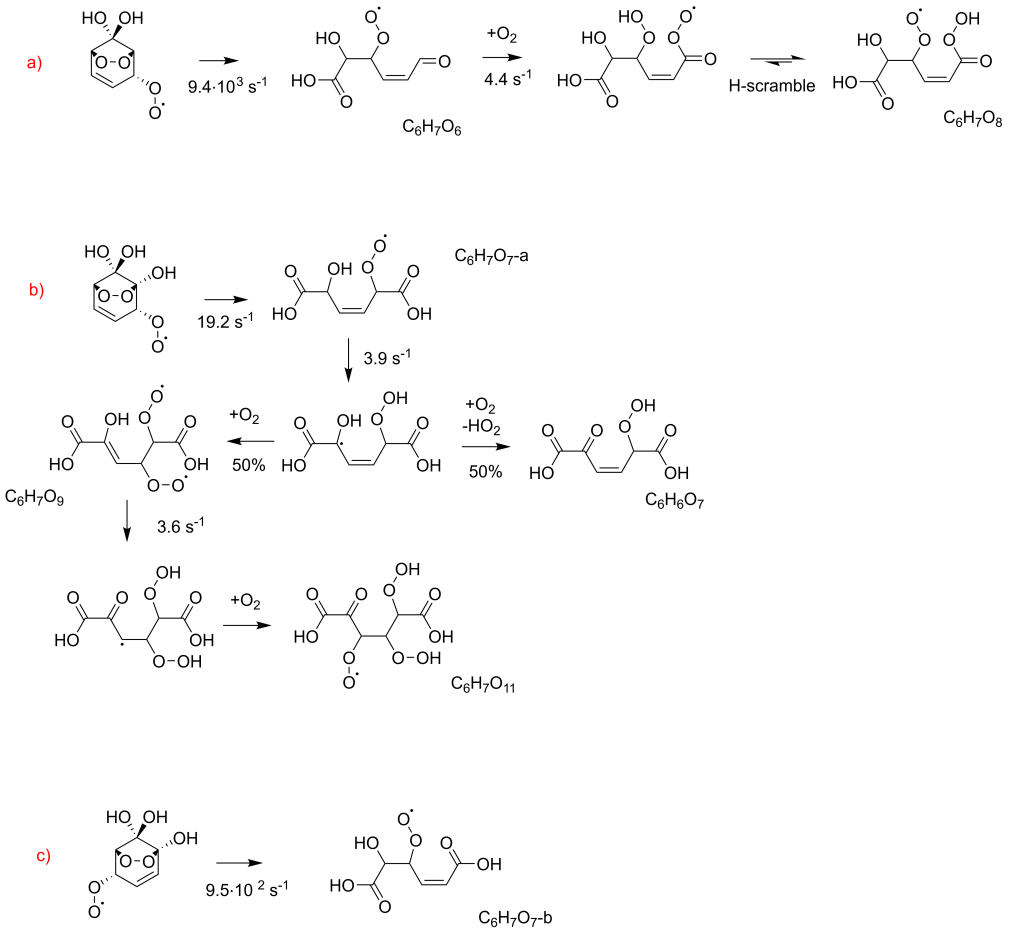

Figure 4. Oxidation schemes of phenol- and catechol-derived geminal diol BPRs. a) Molecular rearrangement of the phenol-derived BPR leads to the formation of compounds with 8 oxygen atoms. b,c) Molecular rearrangement of the two catechol-derived BPRs. One leads to compounds with up to 11 oxygen atoms, while the other is unlikely to oxidize beyond 7 oxygen atoms due to a lack of labile H-atoms.

The possibility of HOM formation via molecular rearrangement of BPRs formed from ortho-position OH addition was considered. Only one molecular rearrangement direction was considered, as the other opening direction leads to the formation of energetically unfavorable geminal diol intermediates. Previously it was found that transition state optimization for structures of this type fails, with the optimization reverting to the acid forming one presented here regardless of the used bond constraints Ojala et al. (2025). The reaction and associated rate coefficients are presented in figure 5. These were found to be too slow to be atmospherically competitive and thus not implemented into the model. However, we note that the molecular rearrangement transition state in 5 a) suffers from some spin contamination (S^2 value of 0.77), indicating higher uncertainties in the calculated rate coefficient.

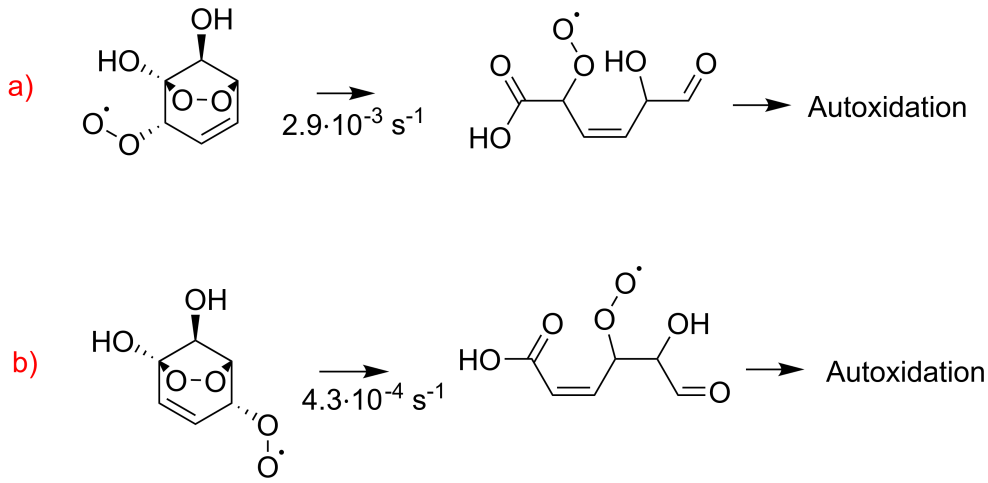

Figure 5. Molecular rearrangement of BPRs formed from ortho-position OH addition. The molecular rearrangement rate coefficients were found to be too slow to be atmospherically competitive

Termination of the autoxidation mechanism is considered through reactions with HO_2 and NO, forming the hydroperoxide or the nitrated equivalent of the formed peroxy radicals, able to partition. The oxidation of intermediate volatile compounds formed during this process (such as the closed-shell species $C_6H_6O_3$) is incorporated into the model by adding its first-generation products to the mechanism using the GECKO-A algorithm (Aumont et al., 2005), allowing for the contribution of these products to SOA formation to be accounted for in the quasi-explicit mechanism. Based on these findings, geminal diol BPR rearrangement pathways and the associated products are incorporated into the quasi-explicit benzene mechanism.

4 Evaluation by comparison to chamber measurements

In order to evaluate the quasi-explicit mechanism developed and its ability to reproduce the formation of SOA, model simulations were compared to experimental results obtained from atmospheric chamber experiments from Choi et al. (2024). The simulations were performed using the SSH-aerosol v2.0 box model, explicitly representing gas–particle partitioning and multiphase chemical processes (Sartelet et al., 2026).

4.1 Presentation of the chemical mechanisms

In the evaluation, several chemical schemes are compared, including the original MCM v3.3.1 mechanism, which serves as the baseline for the developments presented here, and four additional mechanisms designed to isolate the effects of the newly implemented pathways and associated uncertainties. An overview of the chemical mechanisms considered in this work is provided in Table 2. Mech 1 corresponds to MCM v3.3.1 with revised pathways, addition of multi-hydroxylation, peroxy/alkoxy autoxidation, cyclic epoxides formation and BPR rearrangement, as detailed in section 2. In addition to these pathways, the

formation and rearrangement of geminal diol BPRs is taken into account in Mech 2 and Mech 3. The Mech 2 and Mech 3 mechanisms differ in the branching ratios between H-abstraction and OH addition for the OH reaction with catechol, as well as for subsequent reactions involving more highly hydroxylated species formed after further OH addition. Finally, Mech 4 differs from Mech 2 in the endocyclization branching ratios, as described in section 3.2.2.

Table 2. Summary table of the benzene oxidation schemes considered in this study. The *abs.-add.* column describes branching ratios used for OH addition and H abstraction in reactions of phenols with OH. Branching ratio is abbreviated as BR in the header.

Name	Pathways	BR abs.-add.	BR endocycl.	Nb reactions	Nb species
MCM	benzene MCM scheme V3.3.1	-	-	334	135
Mech 1	MCM revised + multi-hydroxylation, autoxidation, epoxides, BPR rearrangement	7 % - 93 %	-	1 494	1 102
Mech 2	Mech 1 + geminal diol BPR rearrangement	7 % - 93 %	50 %	1 766	1 162
Mech 3	Mech 1 + geminal diol BPR rearrangement	30 % - 70 %	50 %	1 766	1 162
Mech 4	Mech 1 + geminal diol BPR rearrangement	7 % - 93 %	10 %	1 766	1 162

4.2 Presentation of the experiments

The set of 16 atmospheric chamber experiments described in Choi et al. (2024) covers a broad range of chemical conditions designed to represent aromatic oxidation and SOA formation. The experiments include two precursors: phenol (experiments 1–8) and benzene (experiments 9–16) and explore variability in NOx levels, as well as the presence, acidity and concentrations in inorganic seed aerosol. For each precursor, the first two experiments are conducted without seed aerosol, the next two experiments include acidic inorganic seeds and the final four employ neutral seed aerosols. Additional details on NOx regimes, seeds nature and meteorological data used are provided in Table 3.

The experiments are conducted over 8 hours under natural daylight, with radical production driven by photolysis. To ensure measurable oxidation and SOA formation within the chamber timescale, the initial precursor concentrations are substantially higher than ambient levels, particularly for benzene, which reacts relatively slowly under atmospheric conditions.

4.3 Model presentation and simulation setup

The simulations were performed using the SSH-aerosol V2.0 box model (Sartelet et al., 2026), a multiphase chemistry–aerosol box model designed to simulate the evolution of gas-phase chemistry and aerosol composition. Aerosol dynamics and multiphase chemical processes are explicitly represented. Semi-volatile organic compounds may partition between the gas, organic and aqueous phases depending on their physicochemical properties and ambient conditions. The quasi-explicit benzene oxidation mechanism is integrated in the model in order to compare simulated SOA formation from benzene and phenol to the chamber experimental results.

Experimental conditions described in Choi et al. (2024) are used to constrain the initial state of the simulations. The simulations are conducted over eight hours with outputs every five minutes. For all benzene-based experiments, as well as experiments

Table 3. Experimental conditions of the phenol and benzene simulations, including NO_x conditions, initial aerosol seeds, and meteorological data.

Phenol exp.	NOx regime	Seed type	Meteo. data [1]	Benzene exp.	NOx regime	Seed type	Meteo. data [1]
1	high	no seed	detailed	9	low	no seed	detailed
2	low	no seed	range	10	high	no seed	detailed
3	high	acidic	detailed	11	low	acidic	detailed
4	low	acidic	range	12	high	acidic	detailed
5	high	neutral	range	13	low	neutral	detailed
6	high	neutral	range	14	high	neutral	detailed
7	low	neutral	range	15	low	neutral	detailed
8	low	neutral	range	16	low	neutral	detailed

[1] Detailed meteorological data correspond to time-resolved temperature and relative humidity provided by the experimental team (Choi et al., 2024). When only a range minimum and maximum values were available, simulations were performed using mean values.

1 and 3 for phenol, meteorological conditions (temperature, humidity) were provided by Choi et al. (2024) and updated in the simulations every five minutes. For the remaining experiments, the temperature and relative humidity are prescribed at each time step using the mean values of the ranges reported in the experiment descriptions. Photolysis rates are calculated based on the location of the chamber and the date of the experiments. An attenuation coefficient is applied to these rates to represent the impact of clouds. This coefficient is adjusted so that the amount of precursor consumed at the end of the simulation corresponds to the one obtained experimentally. Initial precursor concentrations range from 79 ppb to 264 ppb for phenol and from 168 to 325 for benzene. Nitrous acid is introduced as an OH radical source in the benzene experiments only. The initial NOx concentration indicated for each experiment is divided between NO and NO2 to correspond to the initial concentrations presented in the graphs of Choi et al. (2024). The concentrations of inorganic aerosols introduced at the initial state range from 62 to 2201 μg m^{-3} in the phenol experiments and from 10 to 377 μg m^{-3} in the benzene experiments.

Losses on the simulation chamber walls are included using the parameterizations included in SSH-aerosol (Sartelet et al., 2026). Semi-volatile gas-phase compounds undergo reversible wall uptake controlled by kinetic transfer and wall–gas partitioning. The model parameters are set to $\frac{S}{V} = 1.654\ m^{-1}$ for the surface over volume ratio, and to $k_e = 0.1\ s^{-1}$ for the eddy diffusivity coefficient (Huang et al., 2018). Particle losses are treated as irreversible first-order processes accounting for diffusion, settling, and turbulence. Wall-loss rates are determined from compound properties and fixed chamber parameters (geometry and eddy diffusivity), assuming a 104 m^3 chamber. To better represent NOx chemistry, a wall loss parametrization of NO2 representing surface adhesion is implemented in the model following Fiorentino et al. (2021). In this parametrization, the heterogeneous loss of NO2 is represented via a first-order surface uptake process, which depends on an uptake coefficient γ_{NO_2}(assumed to be 4.5×10^{-6} as in Fiorentino et al. (2021)), on the temperature and the ratio surface over volume of the chamber.

4.4 Relative influence of the different pathways

Simulated SOA concentrations obtained for the 16 chamber experiments are shown and compared with measurements in Fig. 6. Results are presented for three chemical schemes: the reference MCM mechanism, the quasi-explicit Mech 1, and the Mech 2 mechanism, which includes geminal diol chemistry. Experimental observations are indicated by stars.

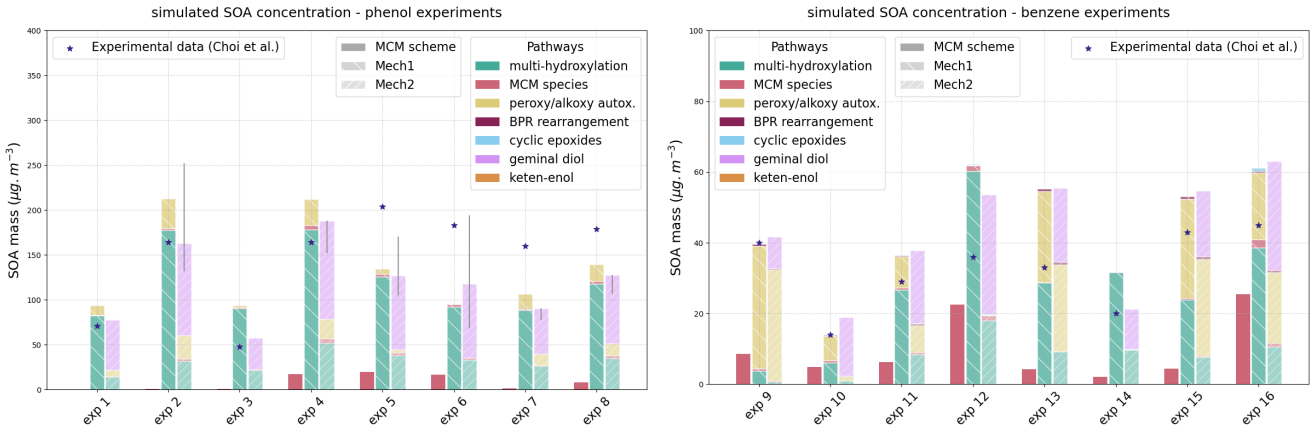

Figure 6. Simulated SOA concentrations obtained with the MCM (left bars for each experiment), Mech 1 (middle bars), Mech 2 schemes (right bars), and comparison to experimental concentrations (stars on the graph). The left panel represents experiments using phenol as the precursor, while the right panel shows experiments using benzene. The sensitivity to meteorological data is indicated by gray error bars when detailed temperature and relative humidity data is missing

Across all 16 experiments, simulations using the MCM scheme systematically strongly underestimate SOA concentrations. These results are consistent with previous studies reporting the lack of representation of HOMs in aromatics chemistry, and motivate the development of quasi-explicit schemes in the first instance. The SOA concentrations are much better represented using the Mech 1 and Mech 2 schemes, within a factor 2 of the experiments, and in most cases within 30 %.

The addition of successive hydroxylation steps, radical autoxidation and geminal diol pathway introduces low-volatility compounds, greatly increasing SOA concentrations. These pathways are dominating SOA formation for all experiments, autoxidation being more important when NOx levels are low (i.e., experiments 9, 13, 15 and 16) and barely represented in high-NOx conditions (experiments 12, 14). The rearrangement pathway from benzene BPR has a low impact on SOA composition due to unfavorable kinetic rate and competition with NO and HO_2 reactions.

Mech 1 tends to slightly overrepresent SOA formation for benzene experiments at low-NOx levels such as in the experiments 13, 15 and 16, in which dimers from accretion reactions in the autoxidation scheme account for a large proportion of the simulated SOA. As observed by Choi et al. (2024), experiments conducted with acidic seeds (3, 4, 11 and 12) are also overestimated, with the successive hydroxylation pathway dominating SOA formation. The formation of SOA from phenol using neutral seeds (experiments 5 to 8) is strongly underestimated, with simulations yielding SOA concentrations that are up to 1.9 times lower than the experimental values (experiment 6). The gas phase contains numerous compounds of intermediate volatility, notably

resulting from the degradation of products formed by the successive oxidation pathway such as C_6 carbonyls and quinones resulting from the reaction of catechol with OH. Uncertainties in the gas/particle partitioning of those compounds may partly explain the discrepancy. The hydration of light aldehydes in the aqueous phase could lead to the formation of additional SOA when seed concentrations are high. Under high relative humidity, this mechanism may partly explain the differences between simulated and observed SOA concentrations in experiments 5, 6, and 8.

The introduction of geminal diol chemistry in Mech 2 significantly modifies SOA formation and composition. For most experiments, the concentrations simulated using Mech 2 better reproduce the amount of SOA obtained experimentally. As with Mech 1, low-NOx concentrations tend to favor autoxidation while successive hydroxylation and its nitrogen derivatives are more prevalent when NOx concentrations are high. In all experiments, the reaction pathway forming geminal diols contributes significantly to the formation of SOA: geminal diol-derived BPRs rearrangement directly competes with the successive hydroxylation pathway and tends to reduce the amount of SOA formed. The addition of this oxidation pathway appears to improve the representation of SOA formation in experiments where Mech 1 overestimate SOA, particularly under conditions in which multi-hydroxylation played a significant role, most notably at high NOx conditions (e.g. experiments 3 and 12).

In addition to total SOA mass, the simulated particle-phase composition provide some additional information on the mechanisms. The proportion of each functional groups is detailed in Supplement S10 and indicate an important increase in the mass fraction of highly oxygenated SOA, particularly hydroperoxides, at the expense of alkyl and hydroxyl groups. This enhanced contribution of hydroperoxides is qualitavely consistent with Borrás and Tortajada-Genaro (2012), who identified hydroperoxides as the dominant functional group in benzene and phenol SOA (see Supplement S11). For comparison with experimental observations on composition, Supplement S11 presents the functional-group composition derived from the benzene oxidation experiments of Borrás and Tortajada-Genaro (2012). These measurements indicate a substantial contribution of oxygen-containing species to the particulate phase, including dicarboxylic compounds, while alkyl groups and carbon–carbon double bonds generally account for smaller fractions of the SOA mass, particularly in the experiments with H_2O_2. The higher degree of oxygenation and the presence of dicarboxylic compounds observed experimentally are more consistent with the composition predicted by Mech 2 than with Mech 1, providing additional support for the inclusion of the geminal-diol oxidation pathway. As hydroperoxides are not similarly dominant in our simulation, their formation might still be under-estimated in our mechanism. Because organic peroxides can contribute to aerosol oxidative potential (Wang et al., 2023a), the differences in SOA composition predicted by Mech 2 may have implications for aerosol toxicity.

4.5 Sensitivity analysis

The simulated concentrations are affected by uncertainties related to model choices and to the representation of environmental conditions. Here, the sensitivity of aromatic oxidation to the competition between OH addition and abstraction pathways is assessed (section 4.5.1), the influence of meteorological conditions (temperature and relative humidity) for experiments where detailed temporal variations are not available (section 4.5.2), the influence of glyoxal gas/particle partitioning (section 4.5.3) and of the endocyclization branching ratio in the geminal diol BPR rearrangement pathway (section 4.5.4). Further studies

conducted on the influence of non-ideality and on nitrophenol saturation vapor pressure are presented in Supplement S6 and S7.

4.5.1 Influence of addition/abstraction branching ratios

To quantify the sensitivity of aromatic oxidation to the competition between OH addition and abstraction, the chemical schemes Mech 2 and Mech 3 described in section 4.1 are compared. For each experiment, the left bars represent the scheme with a 7 % abstraction branching ratio for reactions of benzene and phenols with OH whereas the right bars represent the 30 % abstraction scheme.

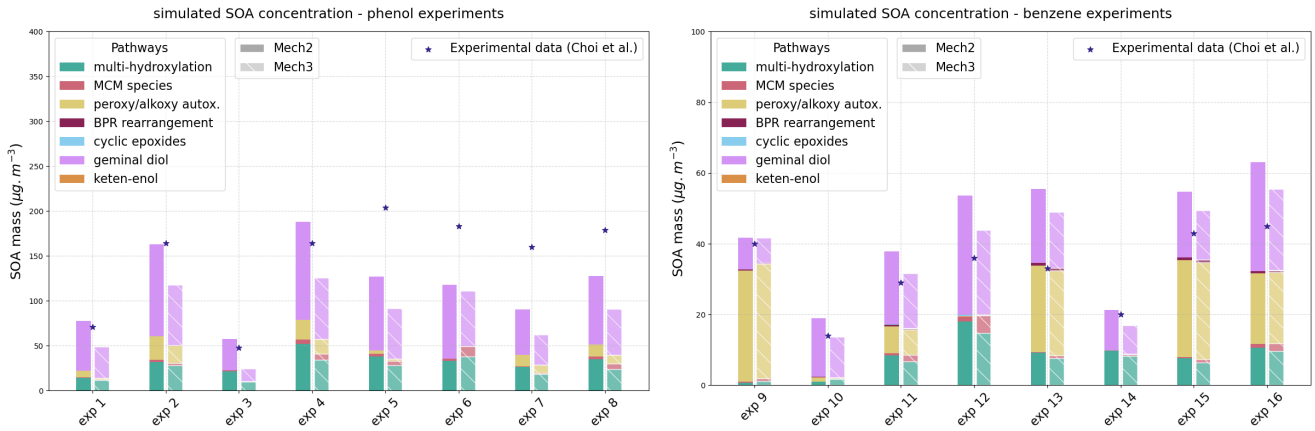

Figure 7. SOA concentrations simulated using Mech 2 and Mech 3 and comparison to experimental concentrations (stars on the graph). The left panel represents experiments using phenol as the precursor, while the right panel shows experiments using benzene.

In Mech 3, the increase in the branching ratio in favor of abstraction leads to a decrease in the amount of SOA formed under most of the experimental conditions. Diverting the initial oxidation toward abstraction lowers the yield of these SOA-forming pathways, especially under high-NOx conditions where abstraction competes with the formation of low-volatility multi-hydroxylated compounds and organonitrates. In low-NOx conditions, SOA formation is mainly driven by autoxidation, peroxy and alkoxy radicals formation and accretion reactions, less dependent on multiple OH additions, lowering the impact of the increased abstraction.

4.5.2 Uncertainty on meteorology

For all benzene-based experiments, as well as experiments 1 and 3 for phenol, the temporal variations of meteorological conditions (temperature, humidity) were provided. However, only mean values were prescribed in the other experiments. To assess the impact of these uncertainties on temperature and humidity on the concentrations, the phenol experiments are simulated using the minimum and maximum temperature and humidity observed during the experiments. The error bars shown in Fig. 6 for experiments 2 and 4 to 8 represent the maximum and minimum SOA concentrations obtained using these extreme

values. Experiments 2, 5, and 6 show the highest sensitivity to meteorological variability, associated with large variations in relative humidity and temperature over the course of the experiments. This sensitivity likely contributes to the underestimation of SOA concentrations in these cases when average meteorological conditions are assumed. Conversely, experiment 7 shows little sensitivity to variations in temperature and relative humidity due to the dry nature of the seeds and the average relative humidity level being representative of extreme conditions.

4.5.3 Influence of glyoxal gas/particle partitioning

In SSH-aerosol, glyoxal can partition through its dissolution into the particle aqueous phase, where rapid hydration shifts the gas–particle equilibrium toward the condensed phase. In addition to this reversible partitioning process, the model includes an irreversible parametrized reaction that converts glyoxal into a non-volatile product. The impact of hydration and of the irreversible parametrized reaction on the simulated concentrations of the chamber experiments are illustrated in Fig. 8.

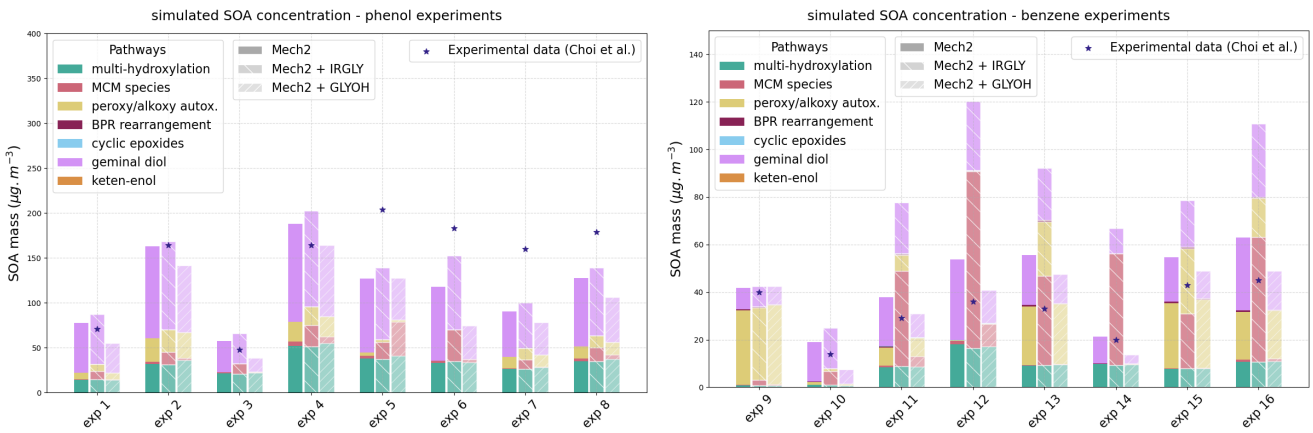

Figure 8. SOA concentrations simulated using Mech 2, Mech 2 + IRGLY taking into account the irreversible partitionning of glyoxal and Mech 2 + GLYOH taking into account glyoxal hydration. The left panel represents experiments using phenol as the precursor, while the right panel shows experiments using benzene.

The implementation of the parameterization for irreversible glyoxal partitioning leads to increased SOA formation under all experimental conditions and to an overestimation of concentrations, especially for benzene experiments conducted in the presence of seeds (Experiments 11 and 12). Experiments using phenol as a precursor also show an increase in SOA concentrations, although to a much lesser extent. Most glyoxal formation results from the decomposition of the benzene bicyclic alkoxy radical, whose formation pathway competes with phenol formation.

On the contrary, the hydration of glyoxal leads to an overall decrease in SOA formation. The formation of hydrated and dihydrated glyoxal increases its uptake in the particulate phase and reduces the availability of glyoxal in the gas phase. This has the effect of reducing the oxidative capacity of the environment as well as the formation of HOMs via benzene oxidation,

since the photolysis of glyoxal in the gas phase leads to the formation of HO_2. This reaction allows for a more accurate representation of SOA concentrations in cases previously overestimated, particularly experiments 4, 13, 15, and 16.

4.5.4 Influence of the endocyclization branching ratio

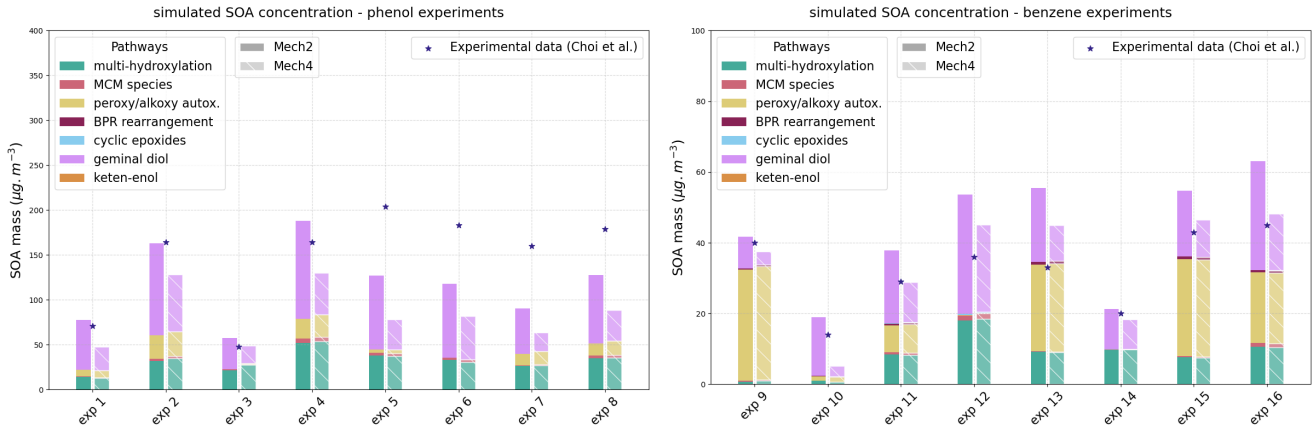

Figure 9. SOA concentrations simulated using Mech 2 and Mech 4. The left panel represents experiments using phenol as the precursor, while the right panel shows experiments using benzene.

Sensitivity simulations are performed using Mech 4 to assess the impact of the branching ratio leading to endocyclization and to compound C6H6O3 in catechol oxidation. Reducing the endocyclization branching ratio from 50 % to 10 % leads to an important decrease in simulated SOA concentrations across most experimental conditions, as seen in Fig. 9. This reduction is due to a lower yield of HOMs as a larger fraction of the oxydated precursor mass is redirected toward C6H6O3, whose first oxidation products are more volatile. The reduction in SOA mass formed is particularly pronounced in experiments where SOA formation is strongly influenced by geminal diol chemistry, for which the reduced endocyclization branching leads to a substantial underestimation of aerosol mass relative to chamber observations. Overall, the comparison indicates that the 50 % approximation on endocyclization branching ratio provides a consistent representation of SOA mass observed experimentally.

5 Reduced scheme for 3D atmospheric modeling

The quasi-explicit oxidation mechanisms developed in this work provide a detailed description of the chemical processes controlling benzene SOA formation but remain computationally too expensive for direct implementation in three-dimensional chemical transport models. It is reduced with the GENerator of reduced Organic Aerosol mechanisms (GENOA), which is an automated framework designed to generate reduced chemical schemes from explicit mechanisms by retaining species and reactions based on their impact on SOA formation. The reduced chemical schemes enable the integration of aerosol-relevant chemistry into air-quality models while maintaining consistency with the detailed quasi-explicit mechanism.

5.1 GENOA model presentation

The GENOA v2 algorithm (Wang et al., 2022) is designed to reduce the size of oxidation mechanisms while maintaining their ability to reproduce SOA formation across a range of VOC precursors and atmospheric conditions, thereby enabling access to detailed SOA composition in 3D simulations. The reduction process relies on several elementary reduction strategies, including removal of species and/or reactions, jumping of an intermediate species, lumping of two similar compounds, and replacement of one by the other. These operations are applied iteratively to the input quasi-explicit scheme and generate a sequence of intermediate simplified mechanisms converging toward a final reduced scheme. After each reduction step, the intermediate mechanism is tested using the 0D box model SSH-aerosol under a set of European atmospheric conditions, to ensure its accuracy compared to the quasi-explicit scheme. User-defined errors control the deviation tolerated from the reference scheme, allowing the generation of reduced mechanisms with different levels of complexity depending on the intended application.

As in Wang et al. (2022) and Sartelet et al. (2024), the GENOA reduction framework relies on a hierarchical evaluation strategy based on three complementary datasets. Throughout the reduction procedure, an eight-condition core dataset is used to evaluate candidate reduced mechanisms, combining six chemically extreme conditions from Wang et al. (2022) and two additional high-NO_x urban conditions from Sarica et al. (2023). To better reflect typical atmospheric variability and test robustness beyond this core set, the evaluation dataset is then expanded to 152 conditions. Finally, a comprehensive testing dataset of 9,433 European conditions is used for the final assessment of the reduced mechanism. For all datasets, box-model simulations are performed over five days with different starting times (12 am, 7 am, 12 pm, and 8 pm) to represent both daytime and nighttime chemistry and to capture SOA formation and aging.

5.2 Mechanism reduction

The reduction is carried out in two successive stages. In the first stage, only four reduction strategies are applied in order to simplify the mechanism while largely preserving its original chemical structure and interpretability. During this stage, the tolerated average error relative to the reference mechanism (ϵ_{mean}) is gradually increased from 0.5 % to 5 %, while the maximum tolerated error (ϵ_{max}) increases from 1 % to 30 %. At the end of the first reduction cycle, the mechanism contains 76 reactions and 70 species, including 35 condensable species. It reproduces SOA mass concentrations with an average error of 1.78 % and a maximum error of 13.32 % over the 9433 testing conditions.

In the second reduction cycle, additional lumping and jumping strategies are introduced with the specific goal of minimizing the number of condensable species. During this cycle, ϵ_{mean} is allowed to increase up to 10 %, while ϵ_{max} remains at 30 %. The second reduction cycle results in a strongly reduced mechanism, retaining only 30 reactions, 28 species, including 12 condensable, which represents 2.6 % of the original reactions and 1.2 % of the original condensable species.

The reduced mechanism resulting from the second reduction cycle reproduces SOA mass concentrations predicted by the Mech 2 mechanism within 3.94 % on average over the 9433 tested conditions, and a maximum error of 22.5 % indicating that the main processes controlling SOA formation from benzene oxidation are well represented and preserved in the reduced scheme. The spatial distribution of the relative error between the reference mechanism Mech 2 and the reduced mechanism is

shown in Fig. 10. Over most locations, errors remain below 5 %. Errors exceeding 10 % are confined to a limited number of locations, while errors above 15 % are rare and are mainly found over North Italy.

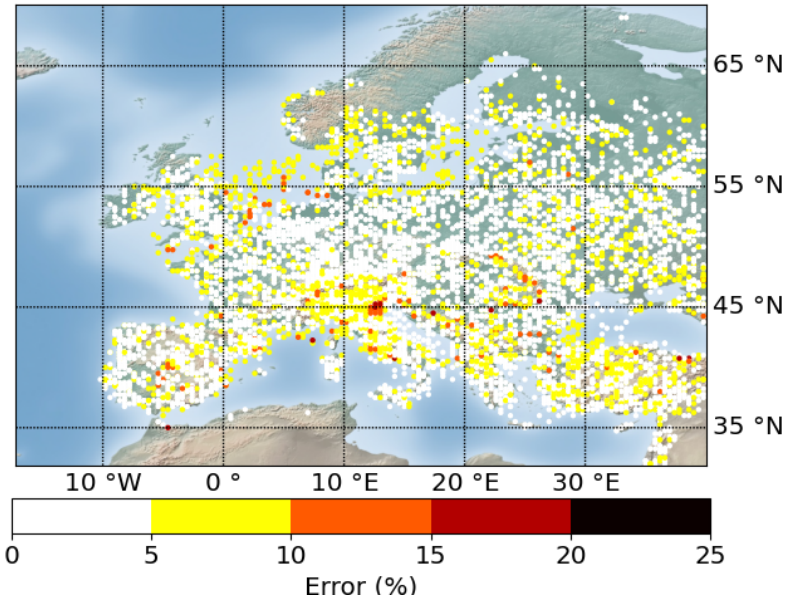

Figure 10. Geographical repartition of the error between the quasi-explicit Mech 2 and the reduced mechanisms.

As illustrated in Fig. 11, the reduced mechanism preserves the main oxidation pathways contributing to SOA formation and identified in section 4. It contains only 12 condensable species. Regarding the oxidation pathways, the successive hydroxylation, the autoxidation of alkoxy and peroxy radicals and the geminal diol BPR rearrangement pathways are retained. Successive hydroxylation processes lead to the formation of BENZ3OH and BENZ4OH. In high-NOx conditions, organonitrates formation is explicitly represented with the formation of nitrocatechol ultimately leading to the highly oxygenated NC4DCO2H or to the NNC_NNC and NPHa_NPHa dimers from accretion reactions. As developed in section 3.2, catechol oxidation and geminal diol BPR rearrangement quickly yields condensable compounds such as species C6H6O4, C6H6O7 and C6H7O12N of the reduced mechanism. Other species represented on the graph result from autoxidation of benzene and phenol BPRs. Termination of the alkoxy and peroxy compounds resulting from the oxidation of phenol BPR is represented through condensable compounds such as C5_uni_O6_O, C5_uni_O6_O, BZo_O9_NO3, BZouni_O6_O and mBZouni_O10_O.

6 Evaluation of the main chemical pathways of benzene and phenol SOA formation

Identifying the major oxidation products formed under atmospherically relevant conditions is essential for improving our understanding of SOA formation and evolution. Beyond the nature of the products formed, their temporal evolution provides key insight into the dominant chemical pathways, allowing rapidly formed species associated with early oxidation stages to be distinguished from compounds that accumulate or persist on longer timescales. To address this, we analyze oxidation product

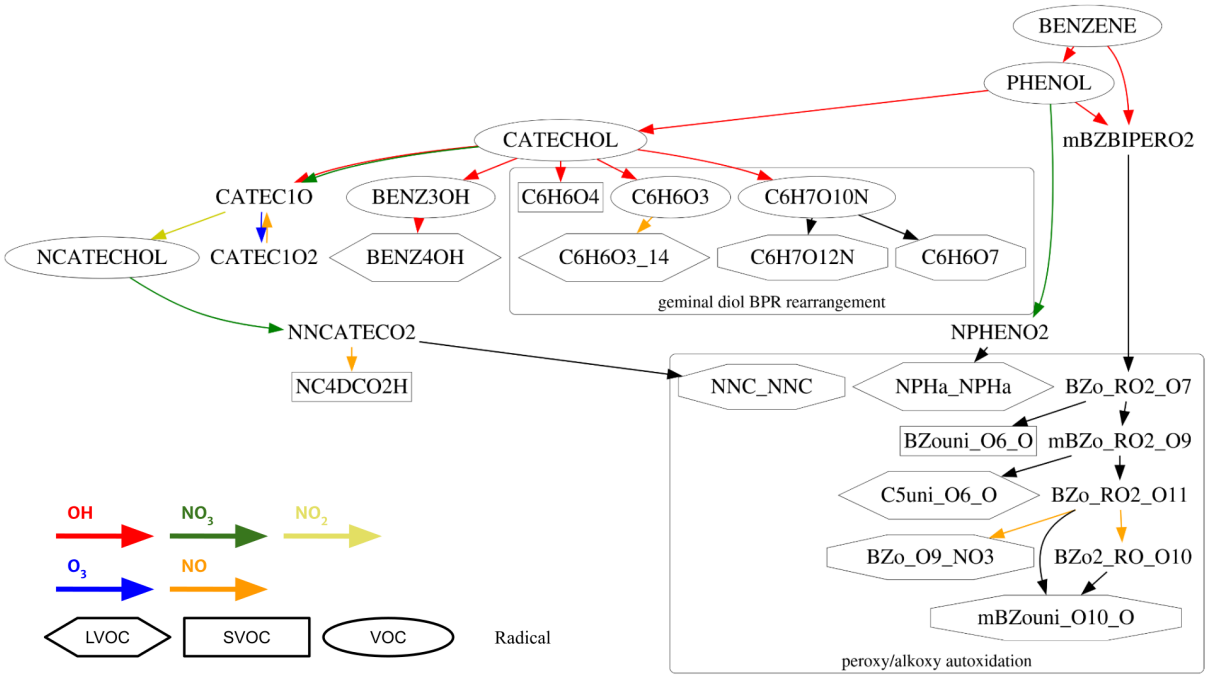

Figure 11. Graphical representation of the reduced scheme. Compounds shown with oval frames are VOCs ($P^{sat} > 10^{-4}\ atm$), rectangular frames are SVOCs ($10^{-4} > P^{sat} > 10^{-9}\ atm$), hexagons are LVOCs ($10^{-9} > P^{sat} > 10^{-13}\ atm$) and frameless compounds are radicals. Arrow color indicates the oxidant involved in the reactions.

distributions using box-model simulations conducted with SSH-aerosol under constant oxidant concentrations representative of either rural or urban conditions. Fig. 12 compares the benzene and phenol SOA composition after short (30 min) and longer (4 h) simulation times in a winter/summer and rural/urban conditions and beginning at 12pm, to assess the compounds that are formed efficiently in the early stages of oxidation and those that dominate the system at later stages.

The simulations show significant contrasts between urban and rural environments and exhibit a strong seasonal dependence. Stronger photochemical activity and higher OH concentrations in summer favor SOA formation via OH addition and geminal diol formation, whereas autoxidation becomes relatively more important in rural environments than in urban settings. It should be noted that, in the present simulations, the peroxy radicals considered are only formed through benzene oxidation. The inclusion of "background" RO_2 radicals from other precursors would increase the contribution of bimolecular RO_2 reactions and could enhance SOA formation. For benzene, in rural conditions and in urban winter conditions, SOA formation is initially dominated by autoxidation, leading to efficient formation of highly oxygenated products at early oxidation times. In winter, reduced photochemical activity induces lower oxidant levels, resulting in less competition for RO_2 self-reactions and intramolecular H-shifts. This leads to a dominant contribution of autoxidation products to SOA mass, even in urban conditions.. In contrast, urban summer environments exhibit an important influence of the geminal diol pathway. Over time, competition

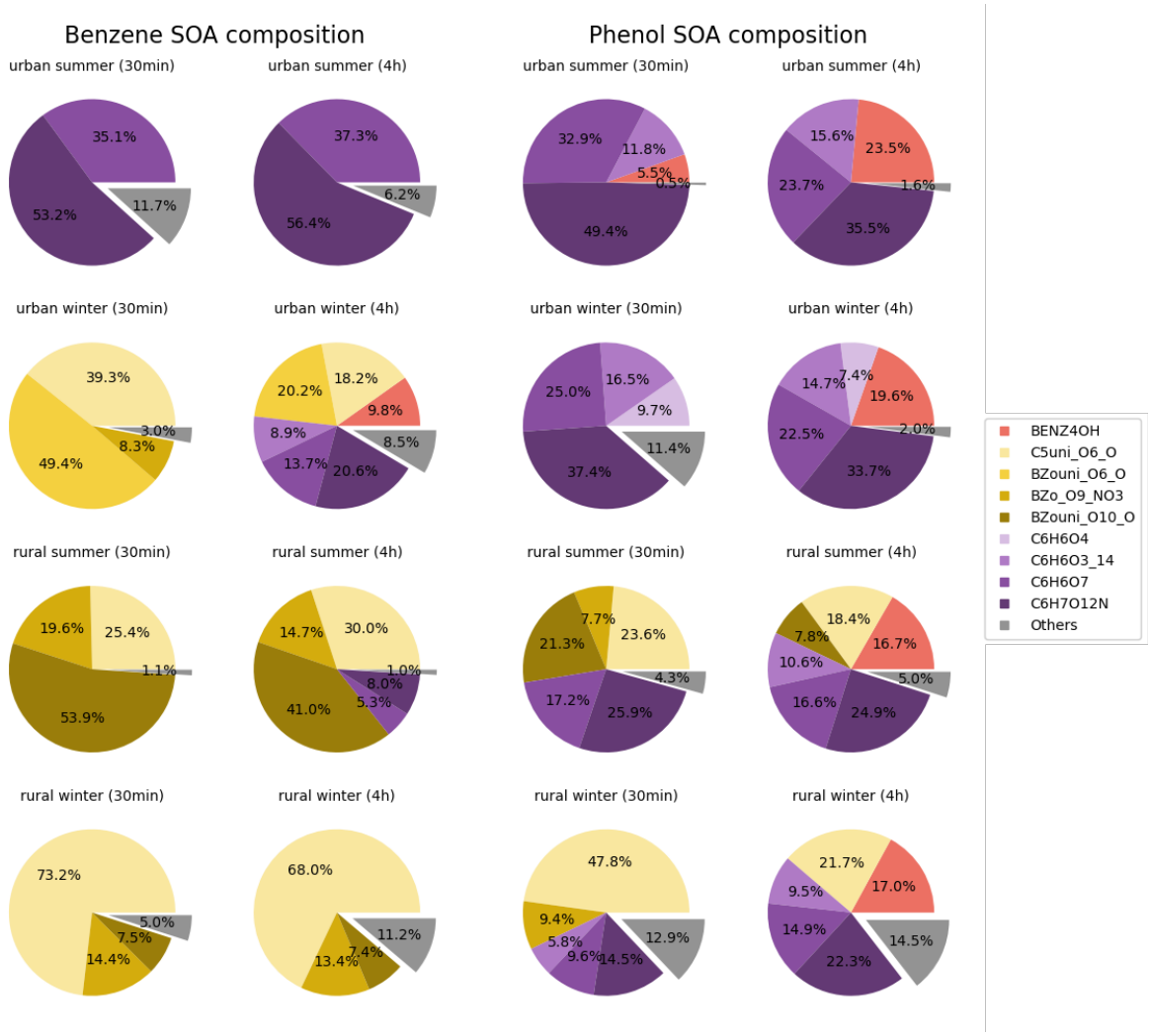

Figure 12. Benzene and phenol SOA composition after short (30 min) and longer (4 h) simulation times in a winter/summer and rural/urban conditions. Compounds representing under 5 % of the SOA mass are aggregated in the "Others" category.

emerges between the direct autoxidation pathways of benzene and the contribution of phenol and catechol via autoxidation along the geminal diol pathway, resulting in an important change in SOA composition between the early stage of oxidation and more aged conditions, especially for urban winter conditions. For phenol, autoxidation is less dependent on seasonal effects, being negligible in the urban environment and accounting for more than 50 % at early stages of oxidation in the rural case. As seen previously for benzene, a substantial fraction of the phenol SOA originates from the geminal diol pathway, with this contribution being particularly pronounced under urban conditions and increasing over time.

7 Conclusions

In this work, we developed a quasi-explicit oxidation mechanism for the formation of benzene and phenol SOAs. This mechanism builds on MCM v3.3.1 and oxidation pathways that are overly simplified or missing are introduced, most notably geminal diol BPRs formation and rearrangement, successive hydroxylation, and peroxy radicals autoxidation, providing a more realistic description of how benzene oxidation progresses toward low-volatility products and SOA formation.

Both comparisons to chamber experiments and simulations in atmospheric conditions show that these pathways play a central role in determining both the concentrations and the molecular composition of benzene and phenol-derived SOAs. Under most conditions, the formation of SOA from benzene is dominated by rearrangement of geminal diol BPRs, accounting on average for 50.0 % of the mass across benzene experiments and 62.8 % for phenol. Successive hydroxylation and peroxy radicals autoxidation, more dependent on NOx and OH conditions, account on average for 19.4 % and 28.5 % of benzene SOA formation, respectively. These added pathways allow for a greater precision on modeled SOA concentration, the benzene MCM mechanism reproducing the experimental values with a mean relative error of 83.2 % compared to 28.2 % for the developed mechanism.

To bridge the gap between chemical detail and large-scale modeling, the quasi-explicit mechanism was reduced using the GENOA algorithm, from 1 772 reactions and 1 160 species to 30 reactions and 28 species. Despite this strong reduction in complexity, the reduced mechanism preserves the three main oxidation pathways controlling SOA formation with an average precision of 3.9 %, making it suitable for implementation in three-dimensional air-quality models while remaining consistent with the underlying chemistry. The representation of intraparticle chemistry remains a source of uncertainty. Recent experiments on biomass-burning organic aerosol indicate that photoinduced radical chemistry within particles can lead to fast atmospheric aging (Zhang et al., 2026). Triplet excited states and other photochemically generated reactive species may be particularly relevant for phenolic compounds, which are abundant in biomass burning emissions.

Code and data availability. The code SSH-aerosol v2.0 is available in the github platform (https://github.com/sshaerosol/ssh-aerosol, last access: 4th June 2026), and on Zenodo: https://doi.org/10.5281/zenodo.14196277 (Sartelet et al., 2026). The chemical mechanisms and raw simulation results used in section 4 are available on Zenodo: https://doi.org/10.5281/zenodo.22897984.

Author contributions. ALB and KS designed the research. ALB, KS, SI and AO contributed to the development of the chemical mechanisms considered in this study. ALB and KS conducted the formal analysis. AO and SI performed and analysed the quantum chemistry calculations. ALB performed the box-model simulations and mechanism reduction, and visualized the data. KS and RC supervised the research. ALB, AO, SI and KS wrote the manuscript draft. ZW, VL, FC and RC reviewed and edited the manuscript.

Competing interests. The authors declare they have no competing interest.

Acknowledgements. We acknowledged fundings from the French National Research Agency (ANR), project SOFORA (grant no. ANR-21-CE01-0019). We thank the Research council of Finland (grant number 355966) for funding and CSC IT Center for Science, Finland, for computing resources. The authors gratefully acknowledge the research team of Jiwon Choi and Myoseon Jang for providing the meteorological data used in this study. We also thank Lauri Franzon for insightful discussions on benzene oxidation kinetics and autoxidation processes.

References

Atkinson, R., Baulch, D. L., Cox, R. A., Crowley, J. N., Hampson, R. F., Hynes, R. G., Jenkin, M. E., Rossi, M. J., Troe, J., and Subcommittee, I.: Evaluated kinetic and photochemical data for atmospheric chemistry: Volume II - gas phase reactions of organic species, Atmos. Chem. Phys., 6, 3625–4055, https://doi.org/10.5194/acp-6-3625-2006, 2006.

Aumont, B., Szopa, S., and Madronich, S.: Modelling the evolution of organic carbon during its gas-phase tropospheric oxidation: development of an explicit model based on a self generating approach, Atmos. Chem. Phys., 5, 2497–2517, https://doi.org/10.5194/acp-5-2497-2005, 2005.

Baan, R., Grosse, Y., Straif, K., Secretan, B., Ghissassi, F. E., Bouvard, V., Benbrahim-Tallaa, L., Guha, N., Freeman, C., Galichet, L., and Cogliano, V.: A Review of Human Carcinogens—Part F: Chemical Agents and Related Occupations, Lancet Oncol., 10, 1143–1144, https://doi.org/10.1016/S1470-2045(09)70358-4, 2009.

Bahadar, H., Mostafalou, S., and Abdollahi, M.: Current understandings and perspectives on non-cancer health effects of benzene: A global concern, Toxicol. Appl. Pharmacol., 276, 83–94, https://doi.org/https://doi.org/10.1016/j.taap.2014.02.012, 2014.

Berndt, T., Scholz, W., Mentler, B., Fischer, L., Herrmann, H., Kulmala, M., and Hansel, A.: Accretion Product Formation from Self- and Cross-Reactions of RO2 Radicals in the Atmosphere, Angew. Chem., Int. Ed., 57, 3820–3824, https://doi.org/10.1002/anie.201710989, 2018.

Bianchi, F., Kurtén, T., Riva, M., Mohr, C., Rissanen, M. P., Roldin, P., Berndt, T., Crounse, J. D., Wennberg, P. O., Mentel, T. F., Wildt, J., Junninen, H., Jokinen, T., Kulmala, M., Worsnop, D. R., Thornton, J. A., Donahue, N., Kjaergaard, H. G., and Ehn, M.: Highly Oxygenated Organic Molecules (HOM) from Gas-Phase Autoxidation Involving Peroxy Radicals: A Key Contributor to Atmospheric Aerosol, Chem. Rev., 119, 3472–3509, https://doi.org/10.1021/acs.chemrev.8b00395, 2019.

Bloss, C., Wagner, V., Jenkin, M. E., Volkamer, R., Bloss, W. J., Lee, J. D., Heard, D. E., Wirtz, K., Martin-Reviejo, M., Rea, G., Wenger, J. C., and Pilling, M. J.: Development of a detailed chemical mechanism (MCMv3.1) for the atmospheric oxidation of aromatic hydrocarbons, Atmos. Chem. Phys., 5, 641–664, https://doi.org/10.5194/acp-5-641-2005, 2005.

Borrás, E. and Tortajada-Genaro, L. A.: Secondary Organic Aerosol Formation from the Photo-Oxidation of Benzene, Atmos. Environ., 47, 154–163, https://doi.org/10.1016/j.atmosenv.2011.11.020, 2012.

Calvert, J., Atkinson, R., Becker, K., Kamens, R., Seinfeld, J., Wallington, T., and Yarwood, G.: The Mechanisms Of Atmospheric Oxidation Of Aromatic Hydrocarbons, Oxford University Press, https://doi.org/10.1093/oso/9780195146288.001.0001, 2002.

Cheng, X., Chen, Q., Jie Li, Y., Zheng, Y., Liao, K., and Huang, G.: Highly oxygenated organic molecules produced by the oxidation of benzene and toluene in a wide range of OH exposure and NOx conditions, Atmos. Chem. Phys., 21, 12 005–12 019, https://doi.org/10.5194/acp-21-12005-2021, 2021.

Choi, J., Jang, M., and Blau, S.: Dual Roles of the Inorganic Aqueous Phase on Secondary Organic Aerosol Growth from Benzene and Phenol, Atmos. Chem. Phys., 24, 6567–6582, https://doi.org/10.5194/acp-24-6567-2024, 2024.

Couvidat, F. and Sartelet, K.: The Secondary Organic Aerosol Processor (SOAP v1.0) model: a unified model with different ranges of complexity based on the molecular surrogate approach, Geosci. Model Dev., 8, 1111–1138, https://doi.org/10.5194/gmd-8-1111-2015, 2015.

Couvidat, F., Debry, E., Sartelet, K., and Seigneur, C.: A hydrophilic/hydrophobic organic (H2O) aerosol model: Development, evaluation and sensitivity analysis, J. Geophys. Res., 117, https://doi.org/10.1029/2011JD017214, 2012.

Crounse, J. D., Knap, H. C., Ørnsø, K. B., Jørgensen, S., Paulot, F., Kjaergaard, H. G., and Wennberg, P. O.: Atmospheric Fate of Methacrolein. 1. Peroxy Radical Isomerization Following Addition of OH and O2, J. Phys. Chem. A, 116, 5756–5762, https://doi.org/10.1021/jp211560u, 2012.

Donahue, N. M., Robinson, A. L., Stanier, C. O., and Pandis, S. N.: Coupled Partitioning, Dilution, and Chemical Aging of Semivolatile Organics, Env. Sc. and Tech., 40, 2635–2643, https://doi.org/10.1021/es052297c, 2006.

Finewax, Z., de Gouw, J. A., and Ziemann, P. J.: Identification and Quantification of 4-Nitrocatechol Formed from OH and NO3 Radical-Initiated Reactions of Catechol in Air in the Presence of NOx: Implications for Secondary Organic Aerosol Formation from Biomass Burning, Env. Sc. and Tech., 52, 1981–1989, https://doi.org/10.1021/acs.est.7b05864, pMID: 29353485, 2018.

Fiorentino, E.-A., Wortham, H., and Sartelet, K.: Combining homogeneous and heterogeneous chemistry to model inorganic compound concentrations in indoor environments: the H^2I model (v1.0), Geosci. Model Dev., 14, 2747–2780, https://doi.org/10.5194/gmd-14-2747-2021, 2021.

Franzon, L., Savolainen, A., Iyer, S., Rissanen, M., and Kurtén, T.: Rapid unimolecular reactions of acyl peroxy radicals: extending the structure–activity relationships, Phys. Chem. Chem. Phys., 27, 12 198–12 210, https://doi.org/10.1039/D5CP01175B, 2025.

Fu, Z., Ma, F., Liu, Y., Yan, C., Huang, D., Chen, J., Elm, J., Li, Y., Ding, A., Pichelstorfer, L., Xie, H.-B., Nie, W., Francisco, J. S., and Zhou, P.: An overlooked oxidation mechanism of toluene: computational predictions and experimental validations, Chem. Sci., 14, 13 050–13 059, https://doi.org/10.1039/D3SC03638C, 2023.

Harrison, M. A. J., Heal, M. R., and Cape, J. N.: Evaluation of the Pathways of Tropospheric Nitrophenol Formation from Benzene and Phenol Using a Multiphase Model, Atmos. Chem. Phys., 5, 1679–1695, https://doi.org/10.5194/acp-5-1679-2005, 2005.

Huang, Y., Zhao, R., Charan, S. M., Kenseth, C. M., Zhang, X., and Seinfeld, J. H.: Unified Theory of Vapor–Wall Mass Transport in Teflon-Walled Environmental Chambers, Env. Sc. and Tech., 52, 2134–2142, https://doi.org/10.1021/acs.est.7b05575, pMID: 29378113, 2018.

Iyer, S., Kumar, A., Savolainen, A., Barua, S., Daub, C., Pichelstorfer, L., Roldin, P., Garmash, O., Seal, P., Kurtén, T., and Rissanen, M.: Molecular rearrangement of bicyclic peroxy radicals is a key route to aerosol from aromatics, Nat. Commun., 14, 4984, https://doi.org/10.1038/s41467-023-40675-2, 2023.

Jacob, D. J.: Introduction to atmospheric chemistry, Princeton University Press, 1999.

Jang, M., Czoschke, N., Lee, S., and Kamens, R.: Heterogeneous atmospheric chemistry by acid-catalyzed particle-phase reactions, Science, 298, 814–7, https://doi.org/10.1126/science.1075798, 2002.

Jenkin, M. E., Saunders, S. M., Wagner, V., and Pilling, M. J.: Protocol for the development of the Master Chemical Mechanism, MCM v3 (Part B): tropospheric degradation of aromatic volatile organic compounds, Atmos. Chem. Phys., 3, 181–193, https://doi.org/10.5194/acp-3-181-2003, 2003.

Jenkin, M. E., Valorso, R., Aumont, B., Rickard, A. R., and Wallington, T. J.: Estimation of rate coefficients and branching ratios for gas-phase reactions of OH with aromatic organic compounds for use in automated mechanism construction, Atmos. Chem. Phys., 18, 9329–9349, https://doi.org/10.5194/acp-18-9329-2018, 2018.

Kanakidou, M., Seinfeld, J., Pandis, S., Barnes, I., Dentener, F. J., Facchini, M. C., Dingenen, R. V., Ervens, B., Nenes, A., Nielsen, C., et al.: Organic aerosol and global climate modelling: a review, Atmos. Chem. Phys., 5, 1053–1123, https://doi.org/10.5194/acp-5-1053-2005, 2005.

Kim, Y., Sartelet, K., and Couvidat, F.: Modeling the effect of non-ideality, dynamic mass transfer and viscosity on SOA formation in a 3-D air quality model, Atmos. Chem. Phys., 19, 1241–1261, https://doi.org/10.5194/acp-19-1241-2019, 2019.

Knap, H. C. and Jørgensen, S.: Rapid Hydrogen Shift Reactions in Acyl Peroxy Radicals, The Journal of Physical Chemistry A, 121, 1470–1479, https://doi.org/10.1021/acs.jpca.6b12787, 2017.

Kroll, J. H. and Seinfeld, J. H.: Chemistry of Secondary Organic Aerosol: Formation and Evolution of Low-Volatility Organics in the Atmosphere, Atmos. Environ., 42, 3593–3624, https://doi.org/10.1016/j.atmosenv.2008.01.003, 2008.

Lan, Q., Zhang, L., Li, G., Vermeulen, R., Weinberg, R. S., Dosemeci, M., Rappaport, S. M., Shen, M., Alter, B. P., Wu, Y., Kopp, W., Waidyanatha, S., Rabkin, C., Guo, W., Chanock, S., Hayes, R. B., Linet, M., Kim, S., Yin, S., Rothman, N., and Smith, M. T.: Hematotoxicity in Workers Exposed to Low Levels of Benzene, Science, 306, 1774–1776, https://doi.org/10.1126/science.1102443, 2004.

Lannuque, V., D'Anna, B., Kostenidou, E., Couvidat, F., Martinez-Valiente, A., Eichler, P., Wisthaler, A., Müller, M., Temime-Roussel, B., Valorso, R., and Sartelet, K.: Gas–particle partitioning of toluene oxidation products: an experimental and modeling study, Atmos. Chem. Phys., 23, 15 537–15 560, https://doi.org/10.5194/acp-23-15537-2023, 2023.

Lin, Y.-H., Zhang, Z., Docherty, K. S., Zhang, H., Budisulistiorini, S. H., Rubitschun, C. L., Shaw, S. L., Knipping, E. M., Edgerton, E. S., Kleindienst, T. E., Gold, A., and Surratt, J. D.: Isoprene Epoxydiols as Precursors to Secondary Organic Aerosol Formation: Acid-Catalyzed Reactive Uptake Studies with Authentic Compounds, Env. Sc. and Tech., 46, 250–258, https://doi.org/10.1021/es202554c, 2012.

Luttkus, M. L., Hoffmann, E. H., Tilgner, A., Wackermann, J., Herrmann, H., and Wolke, R.: URMELL – part II: semi-explicit isoprene and aromatics gasSOA modelling, Environ. Sci.: Atmos., 4, 1413–1433, https://doi.org/10.1039/d4ea00075g, 2024.

Majdi, M., Sartelet, K., Lanzafame, G. M., Couvidat, F., Kim, Y., Chrit, M., and Turquety, S.: Precursors and formation of secondary organic aerosols from wildfires in the Euro-Mediterranean region, Atmos. Chem. Phys., 19, 5543–5569, https://doi.org/10.5194/acp-19-5543-2019, 2019.

Mauderly, J. L. and Chow, J. C.: Health Effects of Organic Aerosols, Inhal. Toxicol., 20, 257–288, https://doi.org/10.1080/08958370701866008, 2008.

Mohr, C., Lopez-Hilfiker, F. D., Zotter, P., Prévôt, A. S. H., Xu, L., Ng, N. L., Herndon, S. C., Williams, L. R., Franklin, J. P., Zahniser, M. S., Worsnop, D. R., Knighton, W. B., Aiken, A. C., Gorkowski, K. J., Dubey, M. K., Allan, J. D., and Thornton, J. A.: Contribution of Nitrated Phenols to Wood Burning Brown Carbon Light Absorption in Detling, United Kingdom during Winter Time, Env. Sc. and Tech., 47, 6316–6324, https://doi.org/10.1021/es400683v, 2013.

Møller, K. H., Otkjær, R. V., Hyttinen, N., Kurtén, T., and Kjaergaard, H. G.: Cost-Effective Implementation of Multi-conformer Transition State Theory for Peroxy Radical Hydrogen Shift Reactions, J. Phys. Chem. A, 120, 10 072–10 087, https://doi.org/10.1021/acs.jpca.6b09370, pMID: 27992191, 2016.

Møller, K. H., Bates, K. H., and Kjaergaard, H. G.: The Importance of Peroxy Radical Hydrogen-Shift Reactions in Atmospheric Isoprene Oxidation, J. Phys. Chem. A, 123, 920–932, https://doi.org/10.1021/acs.jpca.8b10432, 2019.

Nakao, S., Clark, C., Tang, P., Sato, K., and Cocker III, D.: Secondary Organic Aerosol Formation from Phenolic Compounds in the Absence of NOx, Atmos. Chem. Phys., 11, 10 649–10 660, https://doi.org/10.5194/acp-11-10649-2011, 2011.

Odum, J. R., Hoffmann, T., Bowman, F., Collins, D., Flagan, R. C., and Seinfeld, J. H.: Gas/Particle Partitioning and Secondary Organic Aerosol Yields, Env. Sc. and Tech., 30, 2580–2585, https://doi.org/10.1021/es950943+, 1996.

Ojala, A., Iyer, S., Le Bayon, A., Kumar, A., Vinkvist, N., Savolainen, A., Kervinen, A., Sartelet, K., and Rissanen, M.: Secondary organic aerosol formation from sequential oxidation of toluene and cresols, https://doi.org/10.21203/rs.3.rs-7621262/v1, unpublished, 2025.

Orlando, J. J. and Tyndall, G. S.: Laboratory studies of organic peroxy radical chemistry: an overview with emphasis on recent issues of atmospheric significance, Chem. Soc. Rev., 41, 6294–6317, https://doi.org/10.1039/C2CS35166H, 2012.

Pankow, J. F.: An absorption model of gas/particle partitioning of organic compounds in the atmosphere, Atmos. Environ., 28, 185–188, https://doi.org/10.1016/1352-2310(94)90093-0, 1994.

Paulot, F., Crounse, J. D., Kjaergaard, H. G., Kürten, A., Clair, J. M. S., Seinfeld, J. H., and Wennberg, P. O.: Unexpected Epoxide Formation in the Gas-Phase Photooxidation of Isoprene, Science, 325, 730–733, https://doi.org/10.1126/science.1172910, 2009.

Peeters, J. and Nguyen, T. L.: Unusually Fast 1,6-H Shifts of Enolic Hydrogens in Peroxy Radicals: Formation of the First-Generation C2 and C3 Carbonyls in the Oxidation of Isoprene, J. Phys. Chem. A, 116, 6134–6141, https://doi.org/10.1021/jp211447q, 2012.

Pichelstorfer, L., Roldin, P., Rissanen, M., Hyttinen, N., Garmash, O., Xavier, C., Zhou, P., Clusius, P., Foreback, B., Almeida, T. G., Deng, C., Baykara, M., Kurten, T., and Boy, M.: Towards Automated Inclusion of Autoxidation Chemistry in Models: From Precursors to Atmospheric Implications, Environ. Sci.: Atmos., 4, 879–896, https://doi.org/10.1039/D4EA00054D, 2024.

Piletic, I., Edney, E., and Bartolotti, L. L.: A computational study of acid catalyzed aerosol reactions of atmospherically relevant epoxides, Phys. Chem. Chem. Phys., 15, https://doi.org/10.1039/c3cp52851k, 2013.

Pope, C. A., Burnett, R. T., Thun, M. J., Calle, E. E., Krewski, D., Ito, K., and Thurston, G. D.: Lung Cancer, Cardiopulmonary Mortality, and Long-term Exposure to Fine Particulate Air Pollution, J. Am. Med. Assoc., 287, 1132–1141, https://doi.org/10.1001/jama.287.9.1132, 2002.

Priestley, M., Bannan, T. J., Le Breton, M., Worrall, S. D., Kang, S., Pullinen, I., Schmitt, S., Tillmann, R., Kleist, E., Zhao, D., Wildt, J., Garmash, O., Mehra, A., Bacak, A., Shallcross, D. E., Kiendler-Scharr, A., Hallquist, Å. M., Ehn, M., Coe, H., Percival, C. J., Hallquist, M., Mentel, T. F., and McFiggans, G.: Chemical characterisation of benzene oxidation products under high- and low-NOx conditions using chemical ionisation mass spectrometry, Atmos. Chem. Phys., 21, 3473–3490, https://doi.org/10.5194/acp-21-3473-2021, 2021.

Pun, B. K., Seigneur, C., and Lohman, K.: Modeling Secondary Organic Aerosol Formation via Multiphase Partitioning with Molecular Data, Env. Sc. and Tech., 40, 4722–4731, https://doi.org/10.1021/es0522736, 2006.

Reimann, S. and Lewis, A. C.: Anthropogenic VOCs, chap. 2, pp. 33–81, John Wiley & Sons, Ltd, ISBN 9780470988657, https://doi.org/https://doi.org/10.1002/9780470988657.ch2, 2007.

Sarica, T., Sartelet, K., Roustan, Y., Kim, Y., Lugon, L., Marques, B., D'Anna, B., Chaillou, C., and Larrie, C.: Sensitivity of pollutant concentrations in urban streets to asphalt and traffic-related emissions, Environ. Poll., 332, 121 955, https://doi.org/10.1016/j.envpol.2023.121955, 2023.

Sartelet, K., Wang, Z., Lannuque, V., Iyer, S., Couvidat, F., and Sarica, T.: Modelling molecular composition of SOA from toluene photo-oxidation at urban and street scales, Environ. Sci.: Atmos., 4, 839–847, https://doi.org/10.1039/D4EA00049H, 2024.

Sartelet, K., Wang, Z., Kim, Y., Lannuque, V., and Couvidat, F.: Advanced modeling of gas chemistry and aerosol dynamics with SSH-aerosol v2.0, Geosci. Model Dev., 19, 389–421, https://doi.org/10.5194/gmd-19-389-2026, 2026.

Schwantes, R., Schilling, K., Mcvay, R., Lignell, H., Coggon, M., Zhang, X., Wennberg, P., and Seinfeld, J.: Formation of highly oxygenated low-volatility products from cresol oxidation, Atmos. Chem. Phys., 17, 3453–3474, https://doi.org/10.5194/acp-17-3453-2017, 2017.

Sun, H., Trabue, S. L., Scoggin, K., Jackson, W. A., Pan, Y., Zhao, Y., Malkina, I. L., Koziel, J. A., and Mitloehner, F. M.: Alcohol, Volatile Fatty Acid, Phenol, and Methane Emissions from Dairy Cows and Fresh Manure, J. Environ. Qual., 37, 615–622, https://doi.org/10.2134/jeq2007.0357, 2008.

Wang, L., Wu, R., and Xu, C.: Atmospheric Oxidation Mechanism of Benzene. Fates of Alkoxy Radical Intermediates and Revised Mechanism, J. Phys. Chem. A, 117, 14 163–14 168, https://doi.org/10.1021/jp4101762, 2013.

Wang, S., Newland, M. J., Deng, W., Rickard, A. R., Hamilton, J. F., Muñoz, A., Ródenas, M., Vázquez, M. M., Wang, L., and Wang, X.: Aromatic Photo-oxidation, A New Source of Atmospheric Acidity, Env. Sc. and Tech., 54, 7798–7806, https://doi.org/10.1021/acs.est.0c00526, 2020.

Wang, S., Zhao, Y., Chan, A. W. H., Yao, M., Chen, Z., and Abbatt, J. P. D.: Organic Peroxides in Aerosol: Key Reactive Intermediates for Multiphase Processes in the Atmosphere, Chemical Reviews, 123, 1635–1679, https://doi.org/10.1021/acs.chemrev.2c00430, 2023a.

Wang, Z., Couvidat, F., and Sartelet, K.: GENerator of reduced Organic Aerosol mechanism (GENOA v1.0): an automatic generation tool of semi-explicit mechanisms, Geosci. Model Dev., 15, 8957–8982, https://doi.org/10.5194/gmd-15-8957-2022, 2022.

Wang, Z., Couvidat, F., and Sartelet, K.: Implementation of a parallel reduction algorithm in the GENerator of reduced Organic Aerosol mechanisms (GENOA v2.0): Application to multiple monoterpene aerosol precursors, J. Aerosol Sci., 174, 106 248, https://doi.org/10.1016/j.jaerosci.2023.106248, 2023b.

Wang, Z., Couvidat, F., and Sartelet, K.: Response of biogenic secondary organic aerosol formation to anthropogenic NOx emission mitigation, Sci. Tot. Environ., 'accepted', 2024.

Weisel, C. P.: Benzene Exposure: An Overview of Monitoring Methods and Their Findings, Chem.-Biol. Interact., 184, 58–66, https://doi.org/10.1016/j.cbi.2009.12.030, 2010.

Wieser, F., Sander, R., Cho, C., Fuchs, H., Hohaus, T., Novelli, A., Tillmann, R., and Taraborrelli, D.: Development of a Multiphase Chemical Mechanism to Improve Secondary Organic Aerosol Formation in CAABA/MECCA (Version 4.7.0), Geosci. Model Dev., 17, 4311–4330, https://doi.org/10.5194/gmd-17-4311-2024, 2024.

Xu, L., Møller, K. H., Crounse, J. D., Kjaergaard, H. G., and Wennberg, P. O.: New Insights into the Radical Chemistry and Product Distribution in the OH-Initiated Oxidation of Benzene, Env. Sc. and Tech., 54, 13 467–13 477, https://doi.org/10.1021/acs.est.0c04780, 2020.

Zaytsev, A., Koss, A. R., Breitenlechner, M., Krechmer, J. E., Nihill, K. J., Lim, C. Y., Rowe, J. C., Cox, J. L., Moss, J., Roscioli, J. R., Canagaratna, M. R., Worsnop, D. R., Kroll, J. H., and Keutsch, F. N.: Mechanistic study of the formation of ring-retaining and ring-opening products from the oxidation of aromatic compounds under urban atmospheric conditions, Atmos. Chem. Phys., 19, 15 117–15 129, https://doi.org/10.5194/acp-19-15117-2019, 2019.

Zhang, J., Cheung, R. K. Y., Decker, Z. C. J., Surdu, M., Bogler, S., Li, K., Wang, T., Modini, R. L., Slowik, J. G., Pagonis, D., Guo, H., Campuzano-Jost, P., Jimenez, J. L., Coggon, M. M., Gkatzelis, G. I., Warneke, C., Hall, S. R., Ullmann, K., Diskin, G. S., Digangi, J. P., Peischl, J., Holmes, C. D., Zhou, S., Zhang, Q., Bell, D. M., El Haddad, I., and Prevot, A. S. H.: Photoinduced Intraparticle Chemistry Drives the Rapid Atmospheric Oxidation of Biomass Burning Organic Aerosol, Env. Sc. and Tech., 60, 24 206–24 216, https://doi.org/10.1021/acs.est.6c02532, 2026.